공학석사 학위논문

Experimental and Analytical Study of RHS X-Joints under Axial Compression

압축을 받는 각형강관 X형 접합부에 대한 실험 및 해석적 연구

2018년 2월

서울대학교 대학원

건축학과

김 정 현

Abstract

Experimental and Analytical Study of RHS X-Joints under Axial Compression

Kim, Jeong Hyun
Department of Architecture and Architectural Engineering
The Graduate School
Seoul National University

Applying high-strength steel to rectangular hollow section (RHS) joints can bring about many technological advantages from design to erection. However, the application of high-strength steel to RHS joints is forbidden or permitted with high-strength penalty in most representative international standards.

To examine the appropriateness of the strength reduction penalty imposed on high-strength steels, six RHS X-joint specimens fabricated from high-strength and ordinary steels were tested under axial compression. The key parameters of this experimental test included brace to chord width ratios and grade of steels. All high-strength steel specimens exhibited sufficient strength compared to the EC3 strength criteria; their strengths were even higher than the EC3 unreduced nominal strength. Significantly different post-elastic joint behavior was observed depending upon the brace to chord width ratio and grade of steels. It was also found that the formulation of sidewall

buckling strength in current EC3 is inaccurate (too conservative) and needs to be improved.

Although improved strength formula was recently suggested by Becque and Cheng (2016), it is still conservative and inaccurate to evaluate the strength of RHS X-joints fabricated from high-strength steel. A new design formula for RHS X-joint experiencing sidewall buckling was proposed in this thesis. When the new normalized plate slenderness ratio proposed in this study is used in combination with the column curve "c" of EC3, the accuracy and consistency in strength predictions were much improved compared to strength formulae currently available.

Keywords: Rectangular hollow section; X-joints; High-strength steel; Ultimate strength formula; Full scale test

Contents

List of Tables

List of Figures

Chapter 1

Introduction

1.1. Research background

The uses of hollow sections have been increased as the structural efficiencies have become obvious to most structure engineers. Especially as a structural member of column or truss loaded under compression or torsion, hollow sections show outstanding resistant performances due to their characteristics of closed sections.

There are two major types of hollow sections that have been applied to structural members. One is a circular hollow section (CHS) and the other is a rectangular hollow section (RHS). CHSs give an efficient distribution of steel about the centroidal axes, as well as the minimum possible resistance to fluid (CIDECT 1992). However, despite of these advantages, it is not simple to weld circular shapes together that needs a specialized manufacturing. Therefore, RHSs have emerged as a practical alternative.

RHS, one of the major types of hollow sections, is easy to connect their flat faces. Furthermore, trusses fabricated from hollow sections are lighter than their counterparts composed of non-tubular sections. In consequence, the use of RHS as a column or a truss member has been progressively increased.

With those favorable structural features of hollow sections, the application of high-strength steel on those sections could have an opportunity to bring significant reduction of total amount of steel and their self-weight which can give an aesthetic view to the buildings. However, current design standards such as KBC (2016) and AISC (2010) forbid applying the steels whose yield stress exceeds 360 MPa to rectangular hollow section joints. Even Eurocode3 (2005), the only structural standard allowing high-strength steels of which nominal yield stress up to 700 MPa to be applied on RHS joints, suggests that the nominal strengths of RHS joints should be calculated with multiplying the strength reduction factors.

Indeed, these conservative restrictions and penalties are based on weak engineering backgrounds. One of the backgrounds of this limitation is due to less ductile characteristics of high-strength steels. Figure 1.1 shows the comparison between ordinary steel (SM490) and high-strength steel (HSA800). As shown in those curves, ordinary steels show clear yield plateau which could absorb energy without increment of stress while high-strength steel gradually lost its stiffness before reaching at the peak of stress. Moreover, while ordinary steels could undergo quite large deformations after the peak stress, the stress of a specimen fabricated from high-strength steel rapidly decrease until the fracture of material. Therefore, this study was primarily

motivated to investigate the appropriateness of the current strength reduction factors for high-strength RHS X-joints.

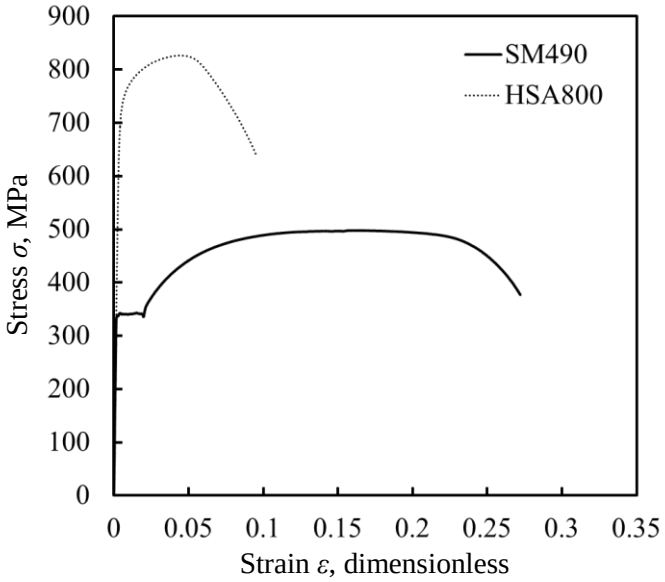

Figure 1.1 Strain-stress relation of ordinary and high-strength steels

1.2. Objectives and scope

For RHS X-joints, two failure modes mainly govern the behavior and the strength. One is a chord plastification which appears at the range of relatively low value of β which is a geometric parameter which represents a width ratio between a brace and a chord, and the other is a chord sidewall buckling which occurs on equal-width (β = 1) RHS X-joints. Thus, in this thesis, these two failure modes are mainly discussed and the others will be briefly introduced.

The main objective of this thesis is to investigate the appropriateness of RHS X-joints strength equations suggested in current design standards, thus,

the strengths of RHS are experimentally and analytically examined. A total of six RHS X-joints specimens were tested under axial compression and compared with key parameters, β and f_y, the yield strength of applied material, to investigate the behavior of joints depending on these parameters.

Rectangular hollow sections are primarily used as truss members loaded in compression or tension, and even bending moments could be transferred by the members. The connection strength decreases when loads (also moments) are applied on a chord member. For this reason, the strengths of RHS joints failure modes; chord plastification and chord sidewall buckling, take into account a chord stress state. As suggested in representative design standards, a strength reduction caused by chord stresses is considered as a chord stress function multiplied in chord plastification and chord sidewall buckling failure modes strength equations derived from theoretical models. In other words, the strength equations could be independently investigated without considering of chord stress states. Furthermore, practically, it is hard to conduct the experiments with considering the chord stress effect simultaneously. Therefore, in this thesis, the chord stresses were neglected in the investigation of the strength and the behavior of RHS X-joints.

1.3. Outline of thesis

This thesis contains five chapters.

Chapter 1 gave an introduction, objectives and scopes of this research work.

Chapter 2 reviews the current design codes and the previous studies on the static behavior of the rectangular hollow section joints.

Chapter 3 shows the experimental testing of RHS X-joints under axial compression.

Chapter 4 proposes a new strength equation of sidewall buckling failure mode derived from a plate buckling model.

Chapter 5 summarizes and gives conclusions of this thesis.

Chapter 2

Review of Design Standards and Previous Studies

2.1. Current design codes

In the 1980s and early 1990s, design guides for statically-loaded welded connections of rectangular hollow sections were mainly developed by the leadership of Wardenier (1982) and CIDECT (1992). The recommendations these works were also included in Eurocode3 (2005). As a consequence, the strength equations and the failure modes of current structural design guides are almost identical to each other.

This section gives the information about a joint configuration, a range of applicability about materials and geometries of RHS joints, the chord stress function which considers the influence of chord stress states affecting the strength of joints and failure modes suggested in current design standards.

2.1.1. Joint configuration

Various types of RHS joints have been applied in different shapes of structures. These types could be classified in two major categories which are called as a uniplanar joint and a multiplanar joint. A uniplanar joint is a joint with members situated in a single plane (see Figure 2.1). K, Y and X joints are general types with an arbitrary value of the angle between a chord and the other members represented by θ_i. (Subscript i represents i^{th} brace. For example, θ_2 is the angle between a chord and 2^{nd} brace.) N and T joints are respectively the special cases of K and Y joints: these types include one brace member perpendicular to a chord member. A DK joint has K joints on chord upper and lower faces. Similarly, a DY joint has Y joints on chord faces.

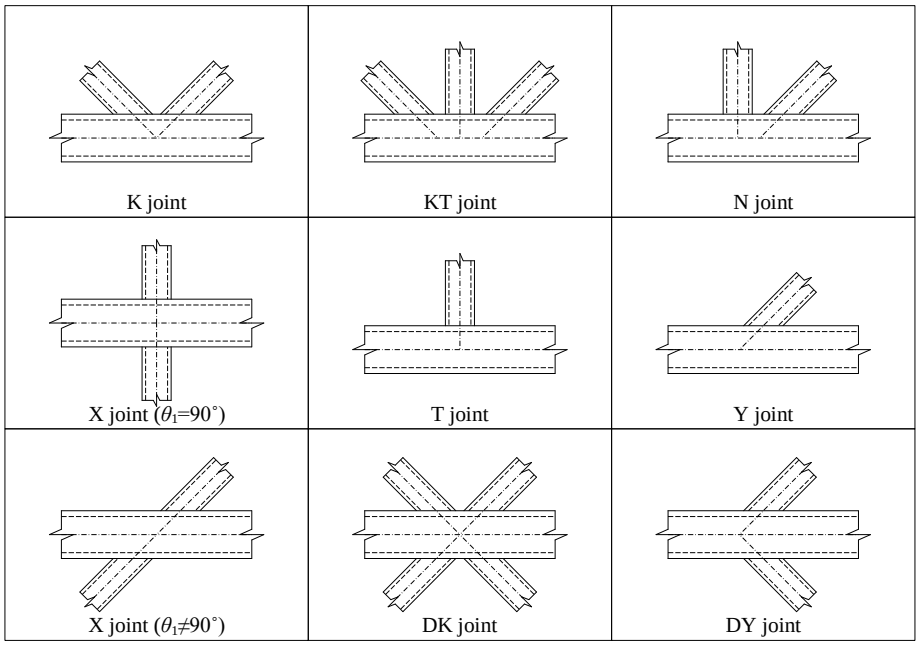

Figure 2.1 Types of uniplanar joints

Otherwise, members of a multiplanar joint are situated in more than one plane. Figure 2.2 shows the configurations for the multiplanar joints.

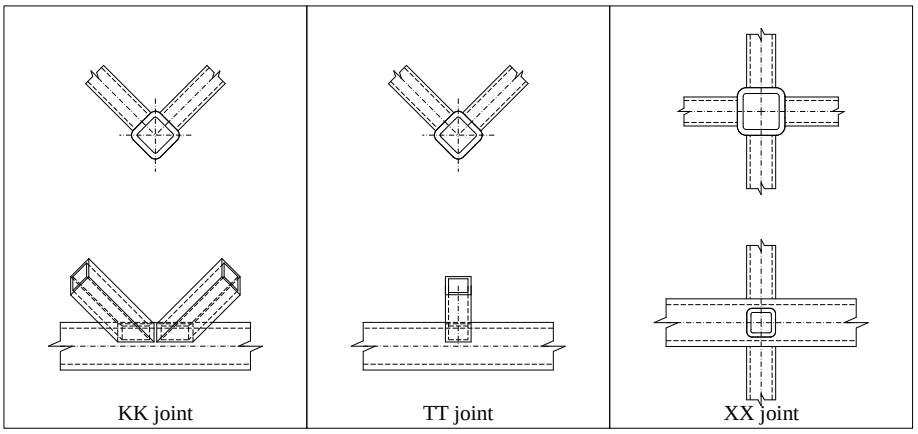

Figure 2.2 Types of multiplanar joints

In Eurocode3 (2005), a configuration of a uniplanar RHS joint is suggested to be determined by a physical appearance of a joint. However, in CIDECT (2009) and AISC (2010), the classification of hollow section joints as K (which includes N), Y (which includes T) or X joints is based on the method of force transfer in the joints. The following descriptions from CIDECT (2009) explain the classification method:

1. When the normal component of a force transferred by a brace member is equilibrated by shear force (and bending moment) in a chord member (see Figure 2.3(a)), the joint is classified as a Y joint. Especially, the joint is classified as a T joint when the brace member is perpendicular to the chord.
2. When the normal force component is transmitted through the chord member and is equilibrated by a brace member (or members) on the opposite side, the joint is classified as an X joint (see Figure 2.3(b)).
3. When the normal component of a force from a brace is essentially equilibrated (within 20%) by the normal force component of another

brace member (or members) on the same side of the joint, the joint is classified as a K joint (see Figure 2.3(c)). The relevant gap is between the primary brace members whose loads equilibrate. A K joint with a brace perpendicular to the chord are classified as a N joint (see Figure 2.3(d)).

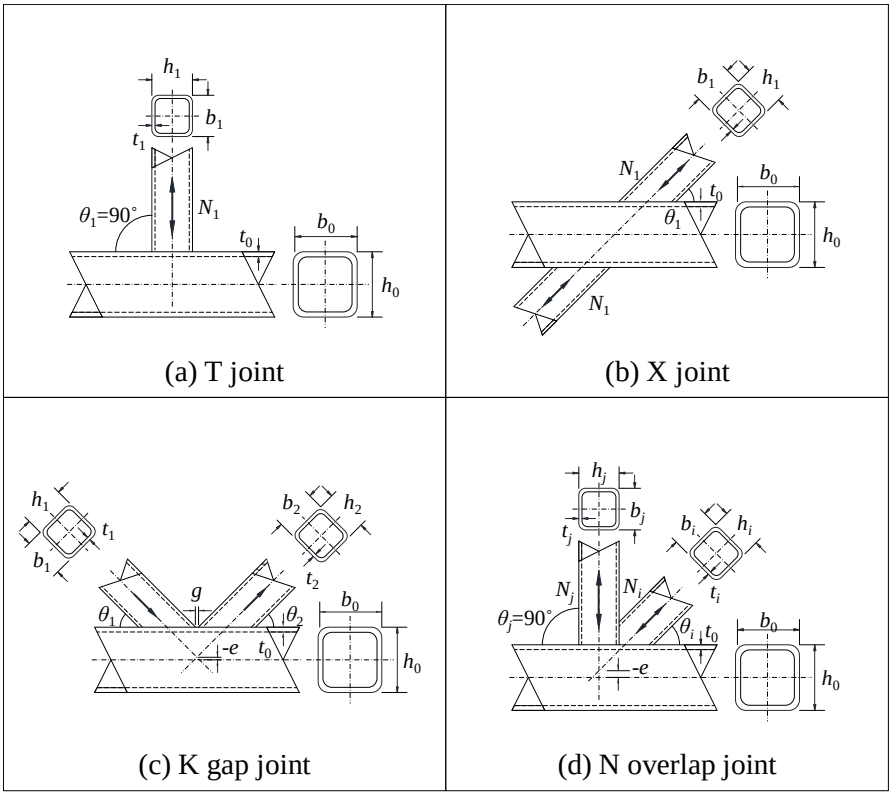

Figure 2.3 Basic joint configurations (T, X and K joints)

In this thesis, RHS X-joints classified as a uniplanar joint will be discussed. Generally, with same magnitude of forces, the strength capacities of joints are critical when the joints are loaded in compression due to their instabilities. Thus, the strength and behavior of RHS X-joints under axial

compression will be investigated as a main topic of this study.

2.1.2. Range of applicability

Material limitations

A yield stress and a yield ratio of high-strength steel of RHS joints are restricted or given penalties by structural standards. Table 2.1 shows their range of applicability. For hollow section joints, AISC (2010) allows applying the steel whose yield strength and yield ratio are within 360 MPa and 0.8, respectively. This limitation implies that the application of high-strength steels, defined as the steel whose yield stress exceeds 355 MPa in CIDECT (2009), to the joints of hollow sections is forbidden.

Table 2.1 Range of applicability: material

Standards	Yield stress (f_y)	Yield ratio (f_y/f_u)
KBC (2016)	f_y < 360 MPa	0.80
AISC (2010)		
CIDECT (2009)	The strength reduction factor should be multiplied as the conditions below: i. 1.0 for f_y < 355 MPa ii. 0.9 for 355 MPa ≤ f_y < 460 MPa	0.80 When yield ratio exceeds 0.8, f_y should be taken as $0.8f_u$
Eurocode3 (2005)	The strength reduction factor should be multiplied as the conditions below: i.1.0 for f_y < 355 MPa ii.0.9 for 355 MPa ≤ f_y < 460 MPa iii.0.8 for 460 MPa ≤ f_y ≤ 700 MPa	i. 0.91 ii.460 MPa ≤ f_y ≤ 700 MPa (from S460 up to S700): 0.95

The joint resistances given in CIDECT (2009) are applicable for those steels with nominal yield strength of up to 355 MPa. The strengths of joints

with the steel whose nominal yield strengths are greater than this value should be obtained from formulae multiplied by 0.9. However, a nominal yield stress should not exceed 460 MPa. Furthermore, if a yield stress exceeds 80% of an ultimate stress of material f_u, the design yield stress used for the prediction of connection strengths should be taken by $0.8f_u$, 80% of the value of the ultimate stress.

For RHS joints fabricated from high-strength steel compatible with S700 whose nominal yield stress is about 700 MPa, Eurocode3 (2005) gives additional rules to allow to apply this steel. The reduction factor of 0.8 should be multiplied in the nominal strength instead of the factor of 0.9 which is used for the strength formula of joints fabricated from the high-strength steel whose yield stress is greater than 355 MPa, but less than 460 MPa. In addition, the applicable range of the yield ratio (f_y/f_u) is expanded up to 0.95.

Geometric parameters

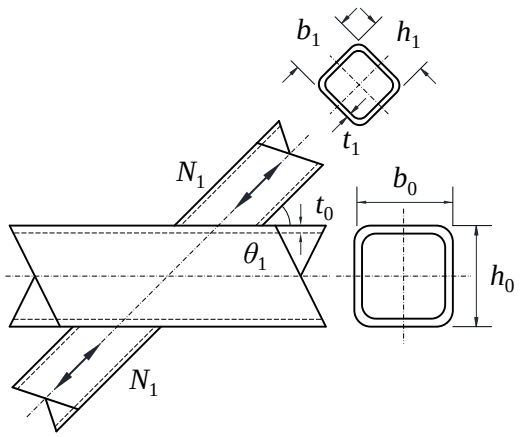

Figure 2.4 Geometric configuration of RHS X-joints

A general geometric configuration of RHS X-joints is shown as Figure 2.4:

where N_1 is a force applied on brace, b is a width of sections, h is a height of sections, t is a thickness of sections and θ_1 is an acute angle between a chord and a brace. Subscript 0 and 1 represent a chord and a brace section, respectively.

Representative design standards such as Eurocode3 (2005), CIDECT (2009) and AISC (2010), prohibit using the RHS X-joints with the geometric parameters which are out of the ranges of applicability to avoid the occurrence of unexpected failure modes.

Table 2.2 Range of applicability for welded joints between RHS brace and RHS chord members

Standards	**AISC (2010)**	**CIDECT (2009)**	**Eurocode3 (2005)**
Brace section slenderness ratio, b_1/t_1 and h_1/t_1	$b_1/t_1 \le 35$, $h_1/t_1 \le 35$ and $b_1/t_1 \le 1.25\sqrt{E/f_{y1}}$, $h_1/t_1 \le 1.25\sqrt{E/f_{y1}}$	$b_1/t_1 \le 40$, $h_1/t_1 \le 40$ and class 1 or 2	$b_1/t_1 \le 35$, $h_1/t_1 \le 35$ and class 1 or 2
Chord and brace section aspect ratio, h_0/b_0 and h_i/b_i	$0.5 \le h_0/b_0 \le 2.0$ and $0.5 \le h_1/b_1 \le 2.0$		
Chord section slenderness ratio, b_0/t_0 and h_0/t_0	$b_0/t_0 \le 35$ and $h_0/t_0 \le 35$	$b_0/t_0 \le 40$, $h_0/t_0 \le 40$ and class 1 or 2	$b_0/t_0 \le 35$, $h_0/t_0 \le 35$ and class 1 or 2
Width ratio, b_1/b_0 and h_1/b_0	$0.25 \le b_1/b_0$ and $0.25 \le h_1/b_0$	$0.1+0.01b_0/t_0 \le b_1/b_0$ but $0.25 \le b_1/b_0$	$0.25 \le b_1/b_0$
Angle between chord and brace, θ_1	$30^\circ \le \theta_1$		

Table 2.2 shows the range of applicability of the section of the RHS X-joints suggested in international structural specifications. For a chord and a brace section, the compact section condition is used to limit their geometries such as section slenderness ratio (b_i/t_i or h_i/t_i, where subscript i represent a chord section with 0 and a brace section with 1). The section classification suggested in Eurocode3 (2005) is shown as Table 2.3.

Table 2.3 Eurocode3 section classification: RHS section subject to bending and compression

Internal compression parts

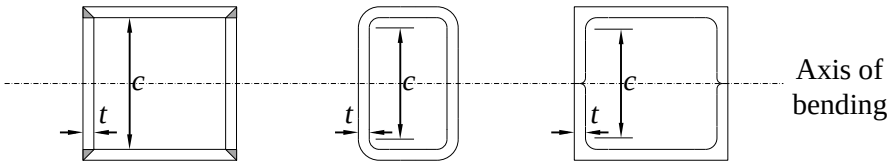

Class		1	2	3		
Part subject to bending		$c/t \le 72\varepsilon$	$c/t \le 83\varepsilon$	$c/t \le 124\varepsilon$		
Part subject to compression		$c/t \le 33\varepsilon$	$c/t \le 38\varepsilon$	$c/t \le 42\varepsilon$		
$\varepsilon = \sqrt{235/f_y}$	f_y, MPa	235	275	355	420	460
	ε	1.00	0.92	0.81	0.75	0.71

2.1.3. Chord stress function

As mentioned in section 1.2, the strength equations of chord plastification and chord sidewall buckling suggested in the representative structural standards reflect the chord stress effect, reducing the strength of joints, by multiplying the chord stress function.

The chord stress functions of Eurocode3 (2005) and AISC (2010) are identical to each other. This function neglects the effect of tensile stress of the chord. Thus, the chord stress function of Eurocode3 (2005) and AISC (2010) is equal to unity which means that there are no stress effects consideration when the chord is in tension.

On the other hand, the compressive stresses induced by the axial load and the bending moment applied on chord section is taken into account to this chord stress function. With small β value, the influence of chord stresses is more sensitively reflected in the chord stress function.

$$Q_{f,\mathrm{E\&A}} = 1.3 + \frac{0.4n}{\beta} \leq 1 \tag{2.1}$$

where $Q_{f,\mathrm{E\&A}}$ is the chord stress function suggested in Eurocode3 (2005) and AISC (2010), n is the factor considering the chord stress induced by applied forces and moments. The equation of n used in equation 2.1 is shown as the following equation:

$$n = \frac{P_0}{F_c A_g} + \frac{M_0}{F_c S} \tag{2.2}$$

where F_c is the available axial strength, A_g is the gross area of the chord, S is the section modulus of the chord, and P_0 and M_0 are the axial load and the moment applied on chord which are determined on the side of the joint that has the higher compression stress, respectively. If the value of n is positive, it represents that the tensile stresses are applied on a chord member while the negative value of n shows that the compressive stresses are acted on a chord

member. Figure 2.5 shows the relationship between the chord stress function of Eurocode3 (2005) and AISC (2010) and factor *n* representing the chord stress state.

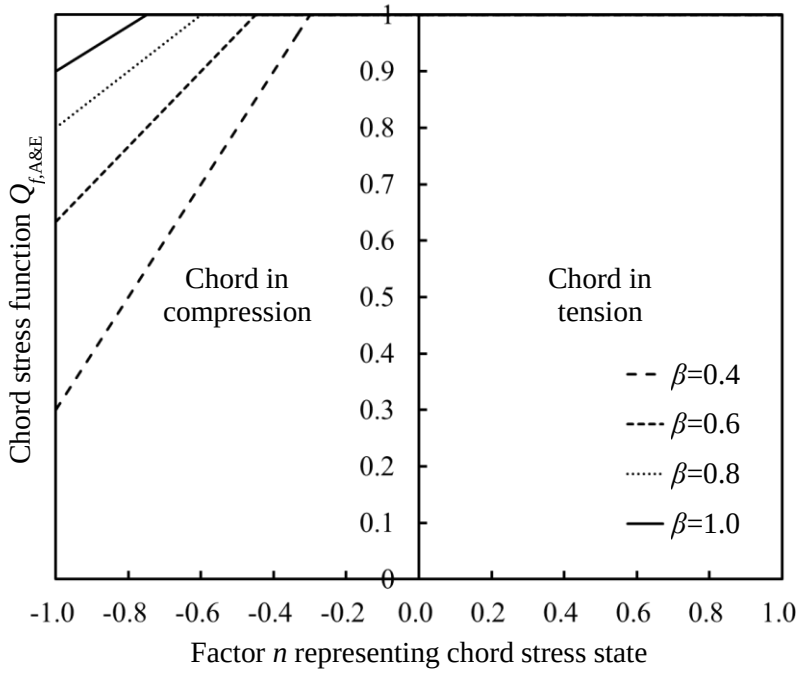

Figure 2.5 Chord stress functions suggested in Eurocode3 (2005) and AISC (2010)

CIDECT (2009) considers the axial compression stress and the moment applied on the chord similar to AISC (2010), but the formula of chord stress function is different from that of Eurocode3 (2005) and AISC (2010). The following equation shows the equation of the chord stress function:

$$Q_{f,\mathrm{CIDECT}} = \left(1 - |n|\right)^{C_1} \tag{2.3}$$

where $Q_{f,\mathrm{CIDECT}}$ is the chord stress function suggested in CIDECT (2009) and $C_1 = 0.6 - 0.5\beta$ for X-joints. This C_1 factor also considers the influence of β

with different form, but shows consideration of β analogous to previous chord stress functions. As the value of β increases, the value of n representing the chord stress state is more insensitively reflected to chord stress function. Figure 2.6 shows the chord stress function of CIDECT (2009), $Q_{f,\mathrm{CIDECT}}$.

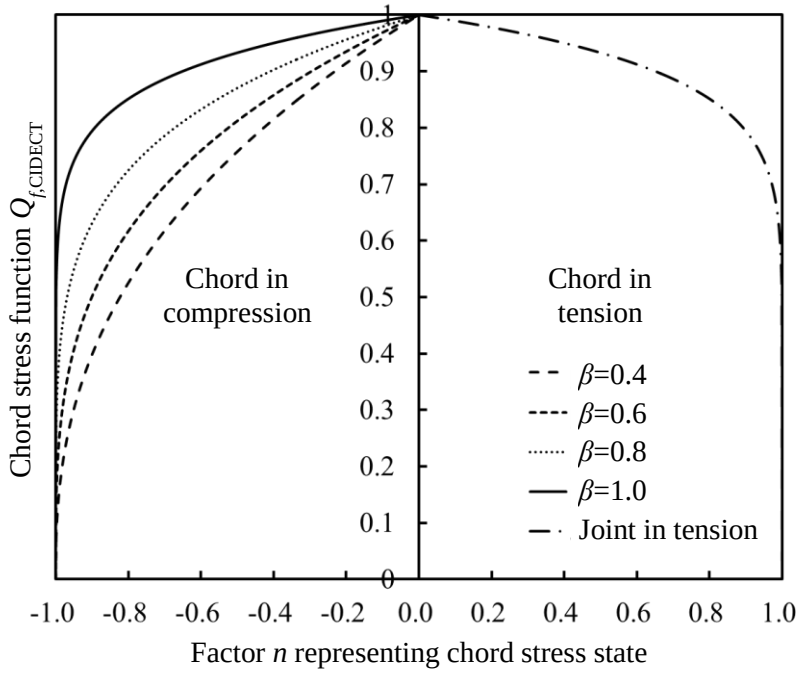

Figure 2.6 Chord stress function suggested in CIDECT (2009)

2.1.4. Failure modes and strength formulae

Representative design standards such as Eurocode3 (2005), CIDECT (2009) and AISC (2010) suggest identical failure modes of RHS X-joints with slightly different form of strength formulae. The failure modes and the strengths of X-joints depend on values of β, a width ratio between a brace and a chord.

A width ratio between a brace and a chord β is one of the important

geometric parameters for RHS X-joints since the force transfer mechanisms of the joints are depending on this parameter. As a value of β becomes larger (becomes closer to unity), the part of chord resisting the most of the forces move from chord upper and lower face to chord sidewalls. Therefore, the governing failure mode of the joint also changes from chord plastification to chord sidewall buckling.

Due to the range of applicability for β, β value could vary in the range of 0.25 to 1. Thus, in the following paragraphs, the failure modes will be introduced depending on the range of β.

1. RHS X-joints with β in the range of 0.25 to 0.85

For the joints with β value greater than 0.25 and less than 0.85, its strength is governed by the limit state of chord plastification.

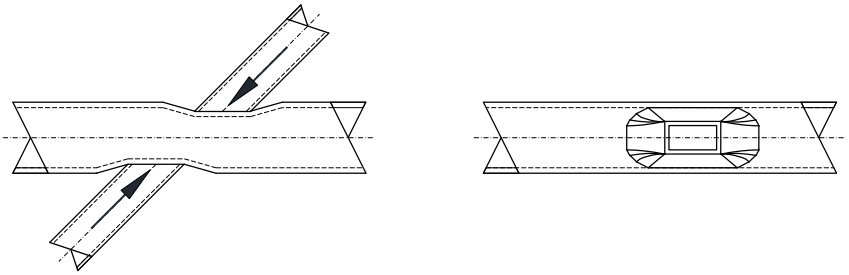

Figure 2.7 Chord plastification failure mode

Figure 2.7 shows the general drawing of chord plastification of X-joints. The strength equation of chord plastification for current design standards is shown as equation 2.4:

$$N_1 \sin\theta_1 = \frac{f_{y0} t_0^2}{1-\beta}\left(\frac{2h_1 / b_0}{\sin\theta_1} + 4\sqrt{1-\beta}\right)\cdot Q_f \qquad (2.4)$$

where N_1 is the force applied on brace, b_0 is the width of chord section, h_1 is the height of brace section, t_0 is the thickness of chord section, f_{y0} is the yield stress of chord, β is the width ratio between brace and chord, θ_1 is the acute angle between a chord and a brace and Q_f is the chord stress function which takes account of the influence of chord longitudinal compressive stresses. Subscript 0 and 1 represent a chord and a brace section, respectively. The only difference of the chord plastification strength equations among the design standards is the chord stress function, as mentioned in previous section. In this study, no chord stresses were applied and considered for RHS X-joints, thus, the value of Q_f is unity.

2. RHS X-joints with β = 1

Chord sidewall buckling

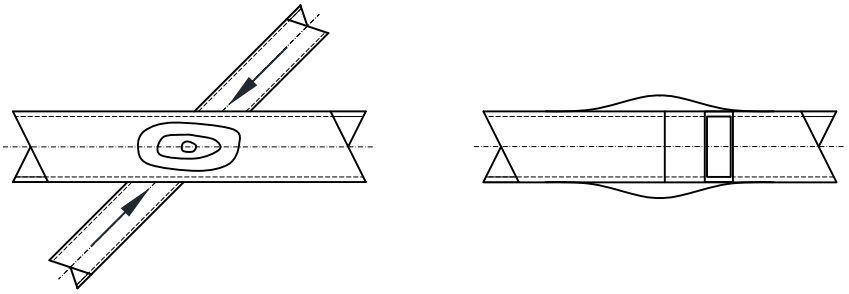

Figure 2.8 Chord sidewall buckling failure mode

RHS X-joints with β = 1, which represents equal-width X-joints, are governed by the chord sidewall buckling. The general illustration of this failure mode is shown in Figure 2.8.

The following equation shows the strength formula of chord sidewall buckling suggested in Eurocode3 (2005) and CIDECT (2009).

$$N_1 = 0.8\chi f_{y0} t_0 \left(\frac{2h_1}{\sin\theta_1} + 10t_0 \right) \cdot Q_f \tag{2.5}$$

where N_1 is a force applied on brace, f_{y0} is the yield stress of the chord, t_0 is the thickness of the chord, h_1 is the height of the brace, θ_1 is the acute angle between brace and chord, Q_f is the chord stress function identical to the function introduced in previous paragraph and χ is the buckling stress reduction factor obtained from EN 1993-1-1 using the relevant buckling curve depending on manufacturing process and grades of steels, and a normalized $\bar{\lambda}$ determined from:

$$\bar{\lambda} = 3.46\left(\frac{h_0}{t_0} - 2 \right) \sqrt{\frac{1}{\sin\theta_1}} \cdot \frac{1}{\pi} \sqrt{\frac{f_{y0}}{E}} \tag{2.6}$$

where h_0 is the height of the chord, t_0 is the thickness of the chord, θ_1 is the acute angle between brace and chord, f_{y0} is the yield stress of the chord and E is the elastic modulus of the material applied to the chord.

In this equation, the factor of 0.8 is multiplied. This factor is used for X-joints while other joints use the value of unity instead. The factor of 0.8 is originated from $1/(\gamma_m\gamma_c)$. γ_m and γ_c are partial safety factors suggested in work of Wardenier (1982), where γ_m is a material factor and γ_c is a factor to take account of the nature of the structure and its behavior and the seriousness of attaining a limit state. For structures with steel, the material factor γ_m have the value of unity. The value of γ_c, 1.25 was set due to the lower plasticity of X-joints.

As mentioned in previous paragraph, there are no chord stresses considered for RHS X-joints in this thesis, thus, the value of Q_f is unity.

Web crippling of RHS

In AISC (2010), web crippling of RHS should be considered as the failure mode of β = 1 RHS X-joints while other design standards suggest to use the sidewall buckling equation for equal-width RHS X-joints. Indeed, web crippling of RHS and chord sidewall buckling are identical failure mode causing a bulging at the mid-height of the chord sidewalls, however, the strength equations were different. The following equation shows the formula of RHS web crippling strength.

$$N_1 \sin\theta_1 = \left(\frac{48 t_0^3}{h_0 - 3t_0} \right) \sqrt{E f_{y0}} \cdot Q_f \tag{2.7}$$

where N_1 is the force applied on brace, h_0 is the height of chord, t_0 is the thickness of chord, E is the elastic modulus of steel, f_{y0} is the yield stress of the chord and Q_f is the chord stress function suggested in AISC (2010).

Chord yield strength and the strength of RHS X-joints with β = 1 suggested in AISC (2010)

In Eurocode3 (2005) and CIDECT (2009), the chord yield strength is considered in the chord sidewall buckling equation for the chord sidewall comprised of stocky sections. For β = 1 RHS X-joints with the normalized slenderness $\overline{\lambda}$ of the chord section less than 0.2, the value of buckling reduction factor χ should be unity. Then the chord sidewall buckling equation shows the strength identical to the chord yielding strength without the factor 0.8 originated from partial safety factors. On the other hand, AISC (2010) only considers the elastic buckling

analogous to web crippling. Thus, to determine the strength of β = 1 RHS X-joints with stocky sidewall sections could be determined as the following equation derived from chord yielding model:

$$N_1 \sin\theta_1 = f_{y0} t_0 \left(\frac{2h_1}{\sin\theta_1} + 15t_0 \right) \tag{2.8}$$

where N_1 is a force applied on brace, θ_1 is the acute angle between the chord and the brace, f_{y0} is the yield stress of the chord, h_1 is the height of the brace and t_0 is the thickness of the chord.

In summary, the strength of β = 1 RHS X-joints suggested in AISC (2010) could be determined by the given function:

$$N_1 \sin\theta_1 = \min\left(\frac{48t_0^3}{h_0 - 3t_0} \sqrt{Ef_{y0}} Q_f,\ f_{y0} t_0 \left(\frac{2h_1}{\sin\theta_1} + 15t_0 \right) \right) \tag{2.9}$$

3. RHS X-joints with β greater than 0.85 less than unity

Mixed failure mode

In the range of β between 0.85 and 1, several failure modes should be considered. One of the failure modes is a mixed mode of chord plastification and chord sidewall buckling. The strength of the joint with β in this range is determined by the linearly interpolated value between the strength of chord plastification at β = 0.85 and the chord sidewall buckling strength at β = 1. The interpolated strength could be expressed by the following equation:

$$N_1 = \frac{N_{1,\beta=1} - N_{1,\beta=0.85}}{1 - 0.85} \cdot (\beta - 0.85) + N_{1,\beta=0.85} \tag{2.10}$$

where $N_{1,\beta=1}$ is the capacity of X-joints with β = 1 calculated by the sidewall buckling strength formula, $N_{1,\beta=1}$ is the capacity of X-joints with β = 0.85 calculated by the chord plastification strength formula and β is a width ratio between brace and chord.

Brace failure

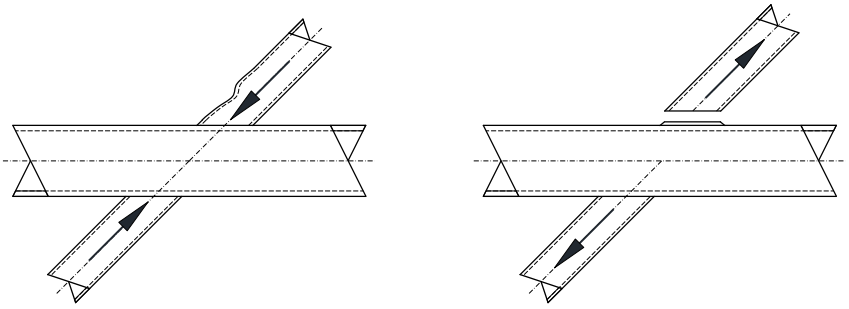

Figure 2.9 Brace failure

Another failure mode is a brace failure. The illustration of brace failure occurred at a RHS X-joint is shown in Figure 2.9. The formula for this failure mode could be expressed as the following equation:

$$N_1 = f_{y1} t_1 \left(2h_1 - 4t_1 + 2b_{eff} \right) \tag{2.11}$$

where f_{y1} is the yield stress of the brace, t_1 is the thickness of the brace, h_1 is the height of the brace and b_{eff} is the effective width for a brace member to chord connection determined from:

$$b_{eff} = \frac{10}{b_0 / t_0} \frac{f_{y0} t_0}{f_{y1} t_1} b_1 \tag{2.12}$$

where b_i is the width of the member, t_i is the thickness of the member and

f_{yi} is the yield stress of the member. Subscript i implies the different member with different numbers: 0 represents a chord member and 1 represents a brace member.

Punching shear failure

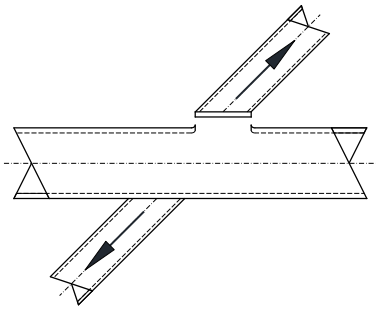

Figure 2.10 Punching shear failure

The other failure mode is a punching shear failure. This failure mode occurs in RHS X-joints with the range of β greater than 0.85 but not exceeding (1-1/γ). The strength equation for punching shear failure suggested in Eurocode3 (2005) is shown as the following equation:

$$N_1 \sin\theta_1 = \frac{f_{y0} t_0}{\sqrt{3}} \left(\frac{2h_1}{\sin\theta_1} + \frac{20}{b_0 / t_0} b_1 \right) \tag{2.13}$$

where h_1 is the height of the brace, b_0 is the width of the chord, b_1 is the width of the brace, respectively, t_0 is the thickness of the chord, θ_1 is the acute angle between brace and chord and f_{y0} is the yield stress of the chord. The factors of 0.6 and 0.58 are used in AISC (2010) and CIDECT (2009), respectively, instead of $1/\sqrt{3}$ suggested in Eurocode3 (2005)

Since brace failure and punching shear failure are the failure modes

occur at brace sections, the chord stress function is not multiplied to the strength equations of these two failure modes.

2.1.5. Design example of RHS X-joints per Eurocode3

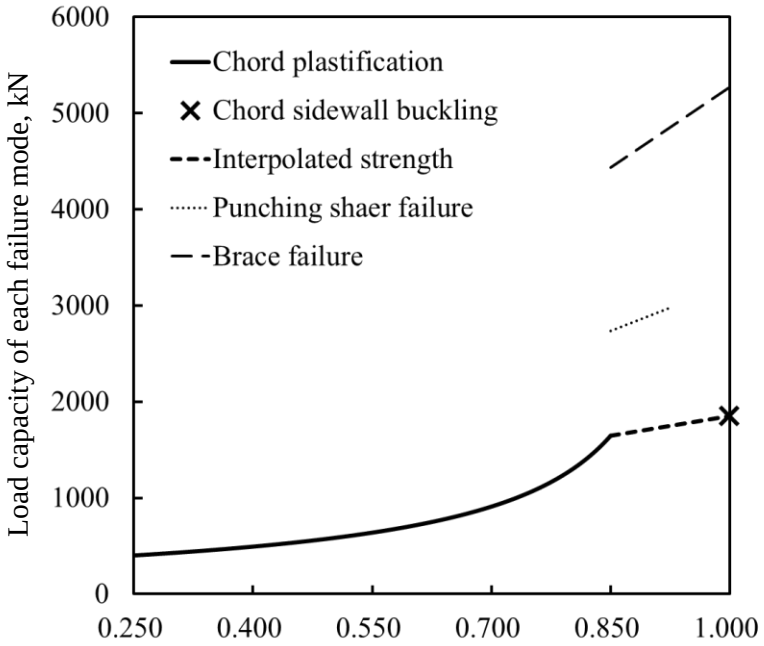

Figure 2.11 EC3 X-joint strength depending on β

As mentioned in previous paragraph, the failure modes and strengths of X-joints changes with the value of β, the width ratio between brace and chord. Figure 2.11 shows an example of an X-joint strength variation depending upon β value. As shown in this Figure, the strengths of failure modes such as chord plastification, chord sidewall buckling and a mixed failure mode mainly governs the strengths of X-joints while the other failure modes show relatively large values of strengths.

As reported in article 2.1.4, the strength formula of a mixed failure mode between chord plastification and chord sidewall buckling is just a linearly interpolated equation of those two strength equations. In this thesis, the method predicting strength of a mixed failure mode by the linearly interpolated formula is not evaluated; however, assuming that this method is reasonable enough, the appropriateness of this method only depends on the accuracy of the strength formula of chord plastification and sidewall buckling. For accurate strength predictions, the theoretical models based on reasonable assumptions should be established. As a consequence, in this thesis, the theoretical models of the chord plastification and chord sidewall buckling will be examined in detail and investigated in respect to the appropriateness of those models.

2.2. Backgrounds of current design standards

2.2.1. Background of chord plastification

Theoretical model

The strength equation of chord plastification is derived from the simplified yield line model. As shown in Figure 2.12, a yield line model with twelve yield lines is established to describe the chord plastification and determine the strength of this failure mode. This theoretical model is based on the assumptions of rigid perfectly plastic material model and small deflection which are general conditions for theoretical models. Due to small deflection assumption, membrane action and strain hardening effects are ignored.

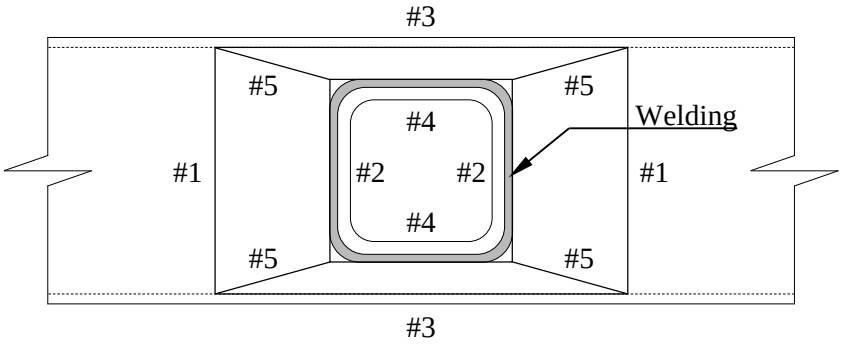

Figure 2.12 Simplified yield line model with twelve yield lines

Application of the Work Method

Figure 2.13 shows the simplified yield line model of chord plastification in detail. The strength equation of chord plastification could be derived from this yield line model with the Work Method.

The Word Method assumes that the potential energy expended by external loads to move the chord face downward must be equal to the energy dissipated (or work done) by rotated yield lines at failure of this model. Therefore, the following equation could be derived:

$$E_{ext} = E_d \Rightarrow \sum\left(N \times \delta\right) = \sum\left(l_i \times \Phi_i \times m_p\right) \tag{2.14}$$

where E_{ext} is the potential energy (work) expended by external load(s), E_d is the energy dissipated by the rotations of yield lines, N is the load(s) acting within a particular region, δ is the vertical displacement of the load(s) N on each region expressed as a fraction of unity, l_i is the length of i^{th} yield line, Φ_i is the rotation of the region about its axis of rotation and m_p is the plastic moment about horizontal axis per unit length which could be expressed the equation of $f_{y0}t_0^2/4$.

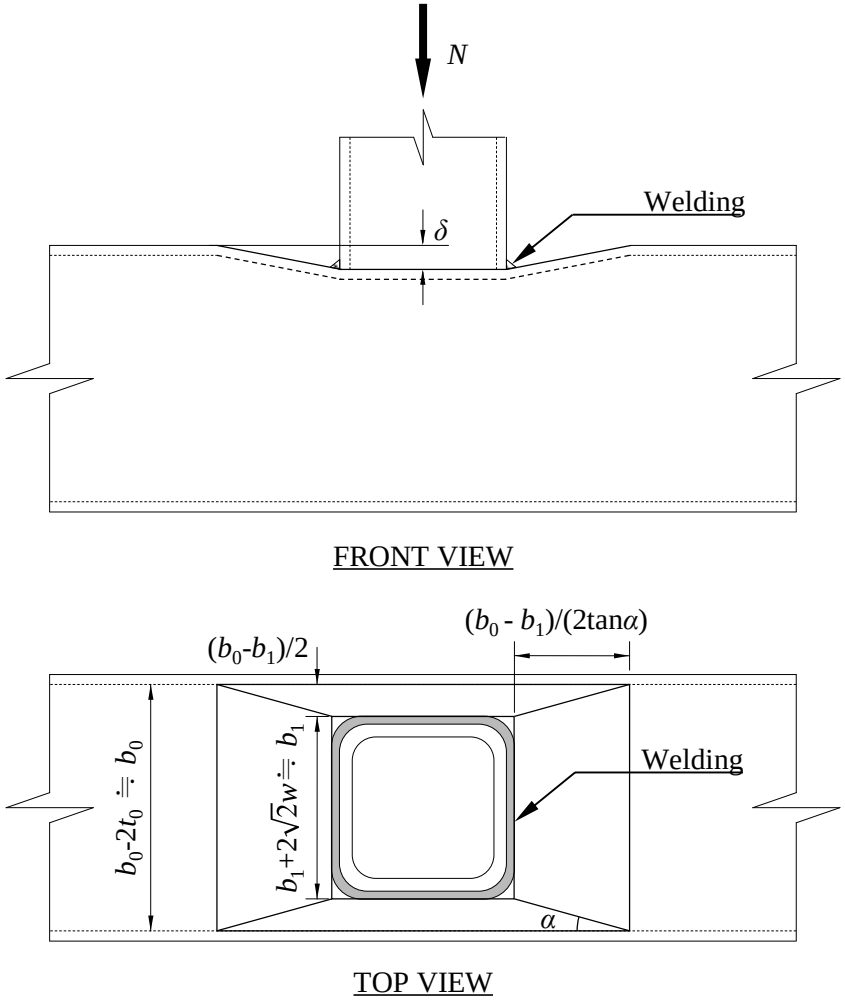

Figure 2.13 Yield line model for RHS joints

Dissipated energy calculation

The total energy participated in the yield lines 1 to 5 is as follows:

Yield lines 1: $E_d = n_1 l_1 \Phi_1 m_p = 2b_0 \cdot \dfrac{2\delta}{(b_0 - b_1)\cot\alpha} \cdot m_p = \dfrac{4\tan\alpha}{1-\beta} \cdot \delta \cdot m_p$

Yield lines 2: $E_d = n_2 l_2 \Phi_2 m_p = 2b_1 \cdot \dfrac{2\delta}{(b_0 - b_1)\cot\alpha} \cdot m_p = \dfrac{4\beta\tan\alpha}{1-\beta} \cdot \delta \cdot m_p$

Yield lines 3: $E_d = n_3 l_3 \Phi_3 m_p = 2\left\{\frac{h_1}{\sin\theta_1} + \frac{2(b_0 - b_1)}{2}\cot\alpha\right\}\frac{2\delta}{b_0 - b_1}\cdot m_p$

$$= \left\{\frac{4\eta}{(1-\beta)\sin\theta_1} + 4\cot\alpha\right\}\cdot\delta\cdot m_p$$

Yield lines 4: $E_d = n_4 l_4 \Phi_4 m_p = 2\frac{h_1}{\sin\theta_1}\cdot\frac{2\delta}{b_0 - b_1}\cdot m_p = \frac{4\eta}{(1-\beta)\sin\theta_1}\cdot\delta\cdot m_p$

Yield lines 5: $E_d = n_5 l_5 \Phi_5 m_p = 4l_5\cdot\left(\frac{\delta}{l_5\cdot\tan\alpha} + \frac{\delta}{l_5\cdot\cot\alpha}\right)\cdot m_p$

$$= 4(\tan\alpha + \cot\alpha)\delta\cdot m_p$$

where $m_p = f_{y0}{t_0}^2/4$ and $\eta = h_1/b_0$

$$\therefore E_d = \sum_{i=1}^{5} n_i l_i \Phi_i m_p = \frac{8m_p\cdot\delta}{1-\beta}\left[\tan\alpha + \frac{1-\beta}{\tan\alpha} + \frac{\eta}{\sin\theta_1}\right] \qquad (2.15)$$

The energy by the external load is $N_1\sin\theta_1\delta$ that is equal to the participated energy in the yield lines which gives:

$$N_1\sin\theta_1\delta = \frac{f_{y0}{t_0}^2}{4}\cdot\frac{8\delta}{1-\beta}\left(\tan\alpha + \frac{1-\beta}{\tan\alpha} + \frac{h_1/b_0}{\sin\theta_1}\right)$$

$$\Rightarrow N_1\sin\theta_1 = \frac{f_{y0}{t_0}^2}{4}\cdot\frac{8}{1-\beta}\left(\tan\alpha + \frac{1-\beta}{\tan\alpha} + \frac{h_1/b_0}{\sin\theta_1}\right) \qquad (2.16)$$

N_1 has minimum value when $\tan\alpha = \sqrt{1-\beta}$ which could be obtained by the partial derivative equation derived from the principle of stationary potential energy given as:

$$\frac{\partial N_1}{\partial\alpha} = 0 \qquad (2.17)$$

Substituting $\sqrt{1-\beta}$ to $\tan\alpha$ yields to the chord plastification strength formula expressed as the following equation:

$$N_1 \sin\theta_1 = \frac{f_{y0} t_0^2}{1-\beta}\left[\frac{2h_1 / b_0}{\sin\theta_1} + 4\sqrt{1-\beta}\right] \tag{2.18}$$

Taking into account the chord stress states by multiplying a chord stress function, it gives the identical equation expressed as Equation 2.4 mentioned in previous chapter.

2.2.2. Theoretical model of chord sidewall buckling

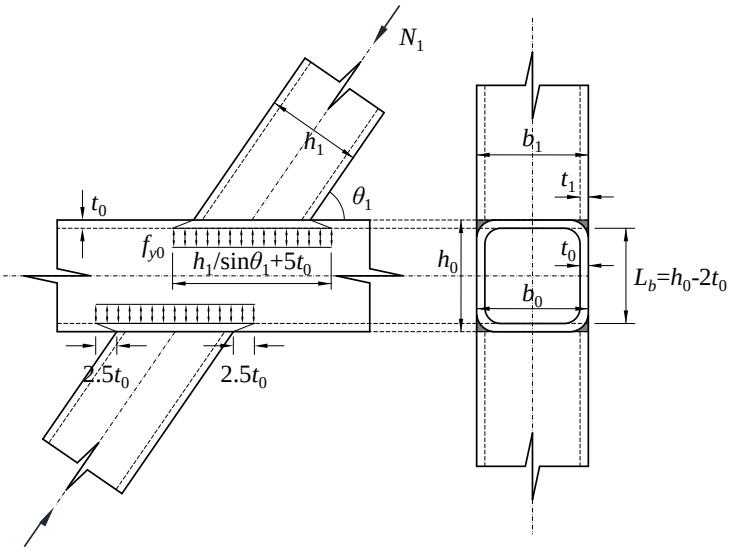

Figure 2.14 Theoretical model: simplistic column buckling approach

A chord sidewall in this model was assumed as a simply supported column which ignores the boundary condition in the longitudinal direction. The stresses transferred from braces are assumed to be distributed into sidewalls with the ratio between a width and a height of 2.5:1 (see Figure

2.14). Then the width of the column b_w could be determined as $h_1/\sin\theta_1+5t_0$.

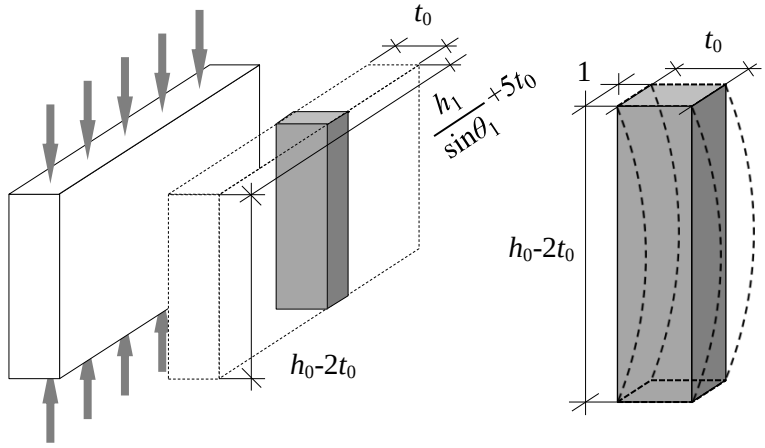

Figure 2.15 Buckling of simplistic column with unit width

If the simplistic column buckles as Figure 2.15, the moment of inertia I could be obtained by a simple equation to calculate a moment of inertia of rectangular sections:

$$I = \frac{bh^3}{12} = \frac{b_w t_0^3}{12} \tag{2.19}$$

where b_w is the width of the column and t_0 is the thickness of the column section. Then the elastic buckling strength of one sidewall assumed as simplistic column is shown as the equation below:

$$N_{cr} = \frac{\pi^2 EI}{L_b^2} = \frac{\pi^2 E b_w t_0^3}{12 L_b^2} \tag{2.20}$$

where b_w is the width of the column, t_0 is the thickness of the column and L_b is the buckling length for this model. From the assumption of this model, the influence of the angle variable is neglected.

The yield strength of a sidewall could be simply obtained as equation 2.21:

$$N_y \sin\theta_1 = f_{y0} A = f_{y0} t_0 b_w \tag{2.21}$$

From this equation, the slenderness ratio used for the chord sidewall buckling could be derived from its definition:

$$\bar{\lambda} = \sqrt{\frac{N_y}{N_{cr}}} = \sqrt{\frac{f_{y0} t_0 b_w}{\pi^2 E b_w t_0^3 / 12 L_b^2}} \approx 3.46\left(\frac{h_0}{t_0} - 2\right) \cdot \frac{1}{\pi}\sqrt{\frac{f_{y0}}{E}} \tag{2.22}$$

Therefore, the sidewall buckling strength equation derived from the simplistic column buckling model is shown as the following equation:

$$N_1 \sin\theta_1 = \chi f_{y0} t_0 \left(\frac{2h_1}{\sin\theta_1} + 10t_0\right) \tag{2.23}$$

where χ is the buckling stress reduction factor obtained from EN 1993-1-1 using the relevant buckling curve and a normalized slenderness $\bar{\lambda}$.

2.2.3. Web crippling strength equation suggested in AISC (2010)

Equation 2.8 which represents the strength formula for AISC (2010) web crippling is repeated here:

$$N_1 \sin\theta_1 = \left(\frac{48 t_0^3}{h_0 - 3t_0}\right)\sqrt{E f_{y0}} \cdot Q_f \tag{2.8}$$

where N_1 is a force applied on brace, h_0 is the height of the chord, t_0 is the thickness of the chord, E is the elastic modulus of steel, f_{y0} is the yield stress

of the chord and Q_f is the chord stress function suggested in AISC (2010).

This equation is originated from the equation of web compression buckling strength expressed as below:

$$R_n = \frac{24t_w^3}{h}\sqrt{Ef_{yw}} \tag{2.24}$$

where h is the clear distance between flanges less the fillet or corner radius for rolled shapes; distance between adjacent lines of fasteners or the clear distance between flanges when welds are used for built-up shapes.

For RHS cross connections, h could be assumed as h_0-$3t_0$ when the bending radius is considered, and the properties (thickness and yield strength) for web could be adjusted to the chord of RHS cross connections. Then, the strength equation of web compression buckling for a sidewall of the chord of RHS cross connection could be expressed as the following equation:

$$R_n = \frac{24t_w^3\sqrt{Ef_{yw}}}{h} = \frac{24t_0^3\sqrt{Ef_{y0}}}{h_0 - 3t_0} \tag{2.25}$$

Since a pair of sidewall of RHS X-joint resists the load transferred from braces, to obtain the web crippling strength of RHS X-joint, equation 2.25 should be doubled. Moreover, the chord stress factor Q_f should be multiplied to consider the effects of chord stress. Then the web crippling strength equation of RHS X-joint could be derived as:

$$N_1 \sin\theta_1 = 2R_n = \frac{48t_0^3}{h_0 - 3t_0}\sqrt{Ef_{y0}} \cdot Q_f \tag{2.26}$$

Background of web crippling strength equation

AISC web crippling strength equation is based on the buckling strength of the simply supported rectangular plate compressed by two equal and opposite forces, introduced in Timoshenko and Gere (1961).

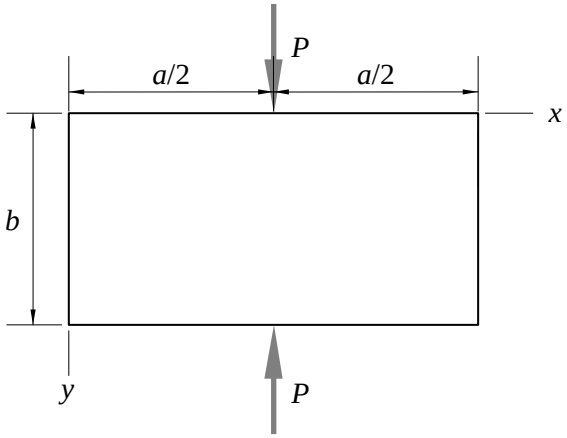

Figure 2.16 Simply supported rectangular plate compressed by two equal and opposite forces

As shown in the Figure above, the length of the plate is represented as the letter *a* and the height of the plate is expressed by the letter *b*. A pair of concentrated compressive forces is loaded at the center of the plate. All edges are regarded to be simply supported. To derive the buckling strength of the plate, the buckled shape of the plate is assumed as following series:

$$w = \sin\frac{\pi y}{b}\sum_{m=1,3,5,\mathrm{L}}^{\infty} a_m \sin\frac{m\pi x}{a} \tag{2.27}$$

Then the elastic buckling strength of the plate model shown in Figure 2.16 could be obtained by the following equation:

$$N_{cr} = \frac{\pi^2 Dab^2 / 2}{\sum_{n=1,3,5,\cdots}^{\infty} \frac{1}{\left((n/a)^2 + (1/b)^2\right)^2}} = \frac{8\pi^2 D / 2\pi b}{\tanh\left(\frac{\pi\beta}{2}\right) - \pi\beta / \left(2\cosh^2\left(\frac{\pi\beta}{2}\right)\right)} \quad (2.28)$$

where β is a/b and D is a flexural rigidity. The buckling strength P_{cr} could be expressed as the equation shown below:

$$N_{cr} = \frac{\pi^2 D}{2b} \cdot f(\beta) \quad (2.29)$$

$$\text{where} \quad f(\beta) = \frac{8/\pi}{\tanh(\pi\beta/2) - \pi\beta / \left(2\cosh^2(\pi\beta/2)\right)}$$

$f(\beta)$ rapidly converges to $8/\pi$ as β increases to ∞. Therefore, the buckling strength for the long plate ($\beta = \infty$) becomes:

$$N_{cr} = \frac{\pi^2 D}{2b}\frac{8}{\pi} = \frac{4\pi D}{b} = \frac{4\pi}{b}\frac{Et_w^3}{12\left(1-\nu^2\right)} \quad (2.30)$$

Chen and Oppenheim (1970) found from observations of the test results in their tests; it appears that far more than in the elastic range, the plastic behavior of the web plate is primarily a local matter and does not depend too much upon geometry and loading of the entire column. Therefore, they suggested that the concentrated load acts only across an effective width, and this width forms a square panel whose size is d_c by d_c. Thus the critical buckling stress becomes:

$$\sigma_{cr} = \frac{N_{cr}}{d_c t_w} = \frac{4\pi}{d_c^2}\frac{Et_w^2}{12\left(1-\nu^2\right)} \quad (2.31)$$

where E is the elastic modulus, d_c is the column web depth between toes of

fillets, t_w is the thickness of the web and v is the Poisson's ratio. From the observation in previous test results, a critical strength of web suggested in this research work is assumed to be proportional to the term $\sqrt{f_y / 36}$ where f_y is yield stress of applied steel in the unit of ksi. Then the modified critical buckling strength could be obtained as:

$$N_{cr}^{*} = N_{cr} \cdot \sqrt{f_y / 36} = \frac{4\pi}{d_c} \frac{Et^3}{12\left(1-\nu^2\right)} \sqrt{\frac{f_y}{36}} = \frac{5562 t_w^3 \sqrt{f_y}}{d_c} \tag{2.32}$$

To fit the most critical test result, the buckling strength equation yields to:

$$N_{cr}^{*} = \frac{5562 t^3 \sqrt{f_y}}{d_c} \approx \frac{4100 t^3 \sqrt{f_y}}{d_c} \tag{2.33}$$

This equation is unbalanced due to the number 36 included in the term $\sqrt{f_y / 36}$, thus, square root of the value of elastic modulus E (about 29000ksi) is multiplied to denominator and numerator of this equation. Then the balanced buckling strength formula yields to the following equation:

$$N_{cr}^{*} = \frac{4100 t^3 \sqrt{f_y}}{d_c} \frac{\sqrt{E}}{\sqrt{E}} = \frac{24 t^3 \sqrt{E f_y}}{d_c} \tag{2.34}$$

AISC (2010) suggests determining the capacity of equal-width RHS X-joints by the minimum value of the strengths corresponding to two different failure modes. These failure modes are the web crippling and the chord local yielding. However, there are no considerations of the RHS X-joints in the range of inelastic buckling. The actual behavior of the joints, in fact, could never be perfectly plastic or elastic. Therefore, some method to take account

of inelastic buckling should be considered to make the strength equation more accurately.

2.3. Previous studies

2.3.1. Research works about high-strength steel

As mentioned in article 2.1.2, the nominal strength of RHS X-joints fabricated from the steel whose yield stress exceeds 355 MPa should be reduced by factor of 0.8 or 0.9 which is determined by the range of yield stress of the steel. However, the mechanical background of this limitation is weak compared to its strict strength penalty.

According to the work of Becque and Wilkinson (2012), most of justification for the reduction factor of 0.9 originates from experimental work conducted on gapped K joints. Kurobane (1981) was first to demonstrate that the ultimate capacity of CHS K gap connections fabricated from S460 steel is in relative terms 18% lower compared to the joints in S235 with the identical geometry. Noordhoek et al. (1996) similarly found that CHS K gap connections of S460 have lower joint strength capacity factors than S235.

However, Puthli et al. (2010) carried out tests on CHS X-joints in S460 and observed that the experimental strength of joints exceeded the nominal strengths calculated without the factor of 0.9. The numerical analysis following experimental results supported this observation. As a consequence, some justification of the strength equation including a reduction factor of 0.9 currently used was insisted to be conservative for X-joints.

Becque and Wilkinson (2012) investigate the results of an experimental program carried out at the University of Sydney to reassess the need for reduction factors multiplied in the strength equations of X and T joints fabricated from C450 steel. The reduction factor of 0.9 should be used for RHS joints in C450 (f_y = 450 MPa) whose nominal yield stress is in the range of greater than 355 MPa, less than 460 MPa. As a result, most of the normalized strengths of tested specimens exceed 1.0. The experimental strengths normalized by nominal strength without the strength reduction factor due to application of high-strength steel also exceed 1.0 or give the values slightly less than unity.

Based on test results, the conclusive evidence is not currently presented to support the inclusion of an additional safety factor of 0.9. Therefore, in this thesis, the appropriateness of the reduction factor of 0.8, multiplied in the strength equation of RHS joints with steel whose yield stress exceeds 460 MPa, will be assessed by experimental results.

2.3.2. Research works about chord sidewall buckling strength

Some researchers mentioned that the strength equation derived from simplistic column buckling model suggested in Wardenier (1982) to predict the strength of RHS X-joint with equal-width is too conservative and inaccurate in their works.

Packer (1984, 1987) carried out experimental studies and suggested a design method to RHS equal-width X-joints. In Packer (1984), a total of 31 cross joint tests (14 of them were RHS to RHS X-joint specimen), all having width ratios β of 1.0, and either plate or RHS branch members welded to an

RHS chord member have been tested under compression. In this research work, the strength equation obtained from CIDECT (1992) and IIW (1981) was evaluated to be far too conservative and inaccurate; the chord sidewall buckling equation suggested by Wardenier (1982) was proved to be an approximate lower bound, but has an extremely high mean value of 1.90, with a very wide scatter (COV = 0.61).

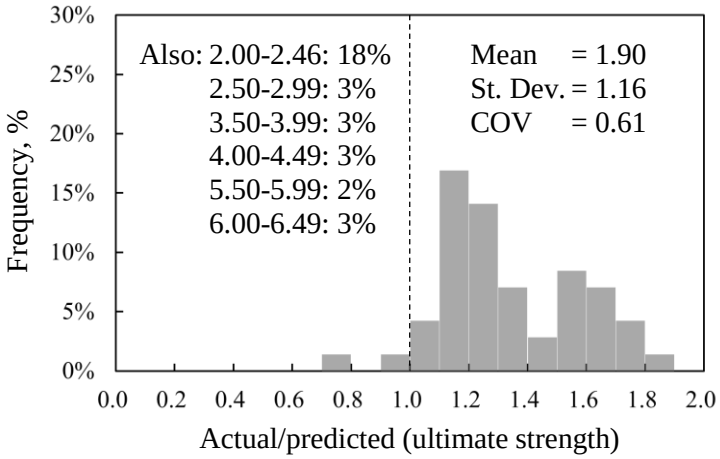

Figure 2.17 Correlation between test results and predictions by Wardenier (1982)

Figure 2.17 shows the correlation between RHS test data collected by Packer and the equation derived by Wardenier (1982). Experimental strength normalized by Wardenier's sidewall buckling equation for 32% of RHS X-joint database specimens were exceeded 2.00 which means that the measured actual strengths are 200% of the strength equation of Wardenier.

As mentioned in previous section, Becque and Wilkinson (2012) tested a total of 15 connections including 4 T-joints and 11 X-joints. Four specimens; X2, X3, X10 and X11 were RHS to RHS X-joints with β = 1. These specimens were failed by chord sidewall buckling and exceeded the predicted

capacity by at least a factor of 2.0. Specimen X2 and X11 were equal-width X-joints with a sidewall slenderness of 50, which is well outside the CIDECT limits ($b_0/t_0 \leq 35$). Nevertheless, these specimens exceeded the capacities predicted by CIDECT by factors of 3.5 to 4.0, the largest margins in their test program.

Due to the inaccuracy of the current design strength equation, an alternative design equation of chord side wall buckling was derived from plate buckling model and validated by experimental (A total of 5 full-scale test specimens) and numerical test results in Becque and Cheng (2016). Specimen X1 through X5 was fabricated from S355 with hot finished square hollow sections of which chord width was 100mm. The alternative equation derived in Becque and Cheng (2016) will be introduced in the following article.

2.3.3. Design equation suggested in Becque and Cheng (2016)

Theoretical model: shape function assumption

A plate with thickness t_0, which extends to infinity on both sides (see Figure. 2.18). The plate was thereby assumed to be made of a linear elastic and homogeneous material.

The loads and boundary conditions were idealized as follows:

1. The distributed load p transferred from the brace sidewall into the chord sidewall was assumed to be uniformly acting over the brace width h_1. The total load N carried by the connection (comprised with two sidewalls) is then given by $N = 2ph_1 = 2\sigma t_0 h_1$ where the stress $\sigma = p/t_0$.

2. The plate is hinged along the longitudinal edges. Thus, no restraints provided the chord upper and lower faces and by the welded connection to the brace members are considered in this model. This is an obviously conservative assumption which could give the underestimated but safe predicted strengths.

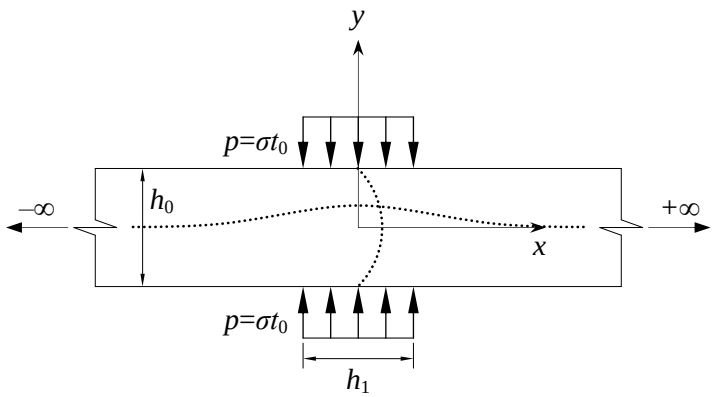

Figure 2.18 Chord sidewall buckling model: plate buckling approach from Becque and Cheng (2016)

A Rayleigh-Ritz method was used to obtain assumed shape function of this plate buckling model. The elastic plate buckling strength could be derived by substituting the assumed shape function; a multiplicative function consisted of a trigonometric function and a truncated Fourier series to a potential energy equation. However, to describe the localized function with sufficient accuracy, large number of Fourier terms would be needed which is not effective to obtain the equation with closed form. Therefore, the exponential Gauss function is instead chosen to represent the longitudinal shape of the buckle. This function is an ideal candidate to capture the localized nature of the failure mode, since its ordinates approach zero almost immediately when leaving a localized area around the origin. When a half-

sine wave solution is also adopted in the transverse direction (across the depth of the chord wall), the proposed deformed shape is expressed by the following function:

$$w = \Delta \cos\left(\frac{\pi y}{h_0}\right) e^{-2Bx^2} \tag{2.35}$$

where w is again the out-of-plane displacement of the plate, while Δ and B are (presently undetermined) parameters. Δ determines the amplitude of the displacements, while B is related to the length of the buckle.

The Gauss function is prominently featured in statistics and from the study of the Gaussian (normal) distribution it is known that only 0.27% of the points in the distribution are more than three standard deviations (3s) removed from the average. The general expression of the Gaussian distribution is shown as equation 2.36:

$$f\left(x, \mu, s\right) = \frac{1}{s\sqrt{2\pi}} e^{-(x-\mu)^2/2s^2} \tag{2.36}$$

where μ is the average and s is the standard deviation, an approximate length of the buckle can be determined as $L_b = 6s$.

Elastic buckling strength derivation

By the principle of stationary total potential energy, the derivatives of the total energy ($U + V$) with respect to s and Δ are set equal to zero:

$$\frac{\partial\left(U+V\right)}{\partial\Delta} = 0 \quad \text{and} \quad \frac{\partial\left(U+V\right)}{\partial s} = 0 \tag{2.37}$$

where U is the elastic strain energy and V is the potential energy of the applied stresses. By solving this system of partial derivative equations, the calculations result could be given in the following equations:

$$s = \frac{h_0}{2\pi}\sqrt{\frac{18}{\sqrt{10}-1}} = \frac{h_0}{2\sqrt{1.186}} = 0.459h_0 \quad \text{and} \quad \sigma_{cr} = 1.346\frac{\pi^2 E}{12\left(1-\nu^2\right)}\frac{t_0^2}{h_0} \tag{2.38}$$

A plate with thickness t_0, which extends to infinity on both sides, the plate was thereby assumed to be made of a linear elastic and homogeneous material. Substituting the value of E = 205000 MPa and ν = 0.3, equation yields to:

$$\sigma_{cr} = (255\times10^3)\frac{t_0^2}{h_0 h_1}\ (\text{MPa}) \tag{2.39}$$

where t_0 is the thickness of the chord, h_0 is the height of the chord and h_1 is the height of the brace. All these variables are in unit of millimeter.

Yield strength of chord sidewalls and slenderness ratio

A chord sidewall yield load can be calculated as the following equation:

$$N_{proposed,y} = 1.2N_y = 1.2\times\left(2\,f_{y0}h_1t_0\right) = 2.4\,f_{y0}h_1t_0 \tag{2.40}$$

where f_{y0} is the yield stress of the chord, h_1 is the height of brace and t_0 is the thickness of the chord. The factor 1.2 thereby takes into account that a small part of the load follows an alternative load path through the chord top and bottom faces and then spreads out into the chord sidewalls.

Therefore, a non-dimensional slenderness can be defined as:

$$\frac{N_{cr}}{N_y}=\frac{\sigma_{cr}}{f_{y0}}=\frac{1}{\lambda^2}=\frac{\left(511\times10^3\right)\times t_0^3/h_0}{2.4\,f_{y0}h_1t_0}=212916.67\times\frac{t_0^2}{f_{y0}h_1h_0}$$

$$\therefore\frac{1}{\lambda^2}=212916.67\times\frac{t_0^2}{f_{y0}h_1h_0}\Rightarrow\lambda=\frac{\sqrt{f_{y0}h_1h_0}}{461.43\times t_0}\approx\frac{\sqrt{f_{y0}h_1h_0}}{500t_0}\qquad(2.41)$$

Using λ above, buckling strength could be calculated by:

$$N_b=\chi N_y=2.4\chi f_{y0}h_1t_0\quad\text{with}\quad\chi=\frac{1}{\phi+\sqrt{\phi^2-\lambda^2}}\le1.0\qquad(2.42)$$

where ϕ is defined as:

$$\phi=\frac{1}{2}\left[1+\alpha\left(\lambda-0.2\right)+\lambda^2\right]$$

In this method, the value of the imperfection factor α is taken as 0.08.

The imperfection factor α of each buckling curve is shown in Table 2.4 and the buckling curves with imperfection factor reported in Table 2.4 are shown in Figure 2.19.

Table 2.4 Imperfection factors for buckling curves

Buckling curve	Becque and Cheng	a_0	a	b	c	d
Imperfection factor α	0.08	0.13	0.21	0.34	0.49	0.76

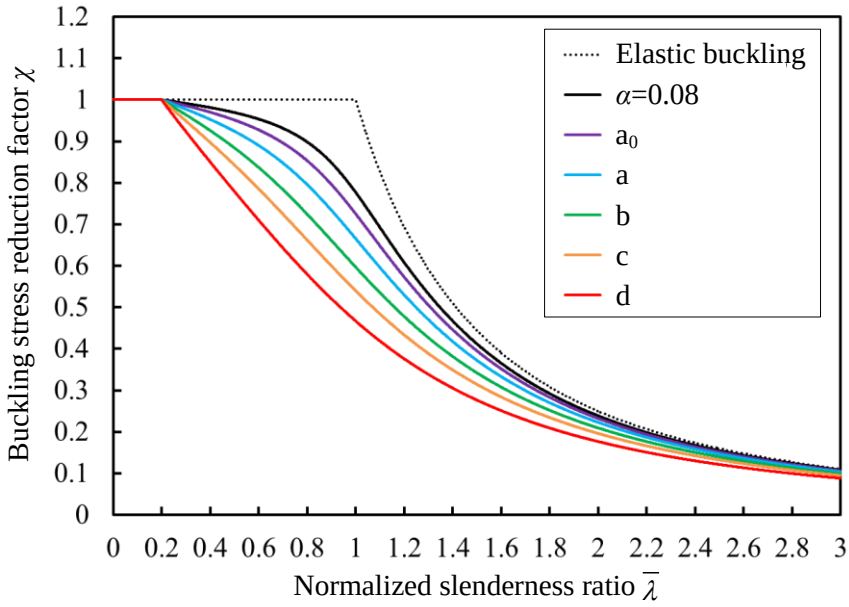

Figure 2.19 Multiple curves suggested in EC3 and Rondal-Maquoi equation with imperfection factor α of 0.08

2.4. Database collected from previous experimental studies

Since the chord sidewall buckling strength equation suggested in Eurocode3 (2005) and CIDECT (2009) was evaluated as a conservative and inaccurate, the experimental test results of RHS X-joints with β = 1 are collected from available previous research works to examine the appropriateness of this equation and the restrictions and penalties on the joints fabricated from high-strength steels.

The following Tables (Table 2.5 through 2.7) show the information of a total of 23 β = 1 RHS X-joint specimens tested under compression in Packer (1984), Becque and Wilkinson (2012) and Becque and Cheng (2016). The

information reported in these Tables include section geometries of the chord section and the brace sections in a format of (width) × (height) × (thickness), measured material properties such as yield stress f_y and ultimate stress f_u of the steels applied to the experimental specimens, and ultimate (peak) strengths of the tested X-joint specimens.

Table 2.5 Database RHS X-joints with β = 1 reported in Packer (1984)

Total: 31 Specimens, β = 1 RHS X-joints: 14 Specimens

Specimen	Chord section (b_0×h_0×t_0), mm× mm× mm	Brace section (b_1×h_1×t_1), mm× mm× mm	θ_1	f_y, MPa	f_u, MPa	N_{exp}, kN
D1121	101.7×77.6×5.08	101.7×77.6×5.08	90°	303	-	403
D1122	77.8×101.8×4.93	77.8×101.8×4.93	90°	358	-	445
D1222	77.8×101.8×4.93	77.8×101.8×4.93	45°	358	-	476
D1322	77.8×101.8×4.93	77.8×101.8×4.93	60°	358	-	459
D2121	304.4×204.1×7.21	304.4×204.1×7.21	90°	406	-	1315
D2122	204.1×304.4×7.21	204.1×304.4×7.21	90°	406	-	1230
D2222	204.1×304.4×7.21	204.1×304.4×7.21	45°	406	-	1675
D3121	203.2×153.6×4.83	203.2×153.6×4.83	90°	392	-	649
D3122	153.6×203.2×4.83	153.6×203.2×4.83	90°	412	-	530
D3221	203.2×153.6×4.83	203.2×153.6×4.83	44°	392	-	693
D3222	153.6×203.2×4.83	153.6×203.2×4.83	44°	412	-	694
D4132	254.1×254.1×9.35	254.1×254.1×9.35	90°	406	-	2183
D4223	254.1×254.1×9.35	254.1×254.1×9.35	45°	406	-	2429
D4323	254.1×254.1×9.35	254.1×254.1×9.35	60°	406	-	2215

Table 2.6 Database for RHS X-joints with β = 1 reported in Becque and Wilkinson (2012)

Total: 15 Specimens, β = 1.0 RHS X-joints: 4 Specimens

Specimen	Chord section ($b_0 \times h_0 \times t_0$), mm× mm× mm	Brace section ($b_1 \times h_1 \times t_1$), mm× mm× mm	θ_1	f_y, MPa	f_u, MPa	N_{exp}, kN
X2	150×250×5	150×150×5	90°	438	514	413
X3	150×150×6	150×150×6	90°	433	502	831
X10	250×350×10	250×250×10	90°	444	534	1770
X11	300×400×8	300×300×8	90°	458	546	1291

Table 2.7 Database for RHS X-joints with β = 1 reported in Becque and Cheng (2016)

Total: 5 Specimens, β = 1.0 RHS X-joints: 5 Specimens

Specimen	Chord section ($b_0 \times h_0 \times t_0$), mm× mm× mm	Brace section ($b_1 \times h_1 \times t_1$), mm× mm× mm	θ_1	f_y, MPa	f_u, MPa	N_{exp}, kN
X1	100.5×100.3×2.92	100.2×100.3×2.73	90°	330	388	176
X2	100.4×100.1×3.84	100.4×100.2×3.69	90°	330	404	302
X3	100.3×99.8×4.89	100.1×99.9×4.70	90°	400	437	373
X4	99.6×99.6×5.80	99.8×99.7×5.46	90°	370	425	560
X5	99.9×99.7×7.92	100.1×99.6×7.68	90°	345	392	783

Chapter 3

Experimental Program

In this chapter, the behavior of high-strength steel RHS (rectangular hollow section) X-joints was investigated through experimental testing. As mentioned in chapter 2, the application of high-strength steel to RHS joints is permitted in EC3 with a joint strength reduction factor of 0.8 or 0.9 depending upon the yield stress of the steel applied to hollow section joints. To examine the appropriateness of the strength reduction penalty imposed on high-strength steels, six RHS X-joint specimens fabricated from high-strength and ordinary steels were tested under axial compression.

3.1. Test program

3.1.1. Key testing parameters

The key parameters were the width ratio β and grade of steels (see Table 3.1).

Note that β values tested were 0.625, 0.85, and 1.0. Two grades of steels, SM490 and HSA800, were chosen to include ordinary and high strength steels. These parameters were determined to investigate the behaviors and strengths of RHS X-joints depending on the grades of steels and the value of β. For this test program, the value of θ_1, the acute angle between the chord and the braces was not considered.

Table 3.1 Experimental program of RHS X-joints

Specimen	Angle between chord and brace, °	Chord width, mm	Brace width, mm	Grade of steel
X90–325–0.625–26.7	90	400	250	SM490
X90–650–0.625–26.7				HSA800
X90–325–0.850–26.7	90	400	340	SM490
X90–650–0.850–26.7				HSA800
X90–325–1.000–26.7	90	400	400	SM490
X90–650–1.000–26.7				HSA800

The identification of specimens was conducted as the rule explained by an example. For X90–650–0.625–26.7 specimen, the character X means that the specimen is classified as X-joints, the number 90 stands for the angle between the chord and the brace, the number 650 shows the yield stress of the steel applied to the specimen in MPa unit, 0.625 shows the value of β, the width ratio between braces and a chord and 26.7 is the value of chord

slenderness ratio represented as the symbol $2\gamma = b_0/t_0$.

3.1.2. Drawings of specimens

Figure 3.2 through 3.4 shows the geometries of all specimens conducted for experimental tests. A length of a chord is 2500 mm and lengths of braces are 600 mm which is about 1.5 times of the largest width of the brace, 400 mm.

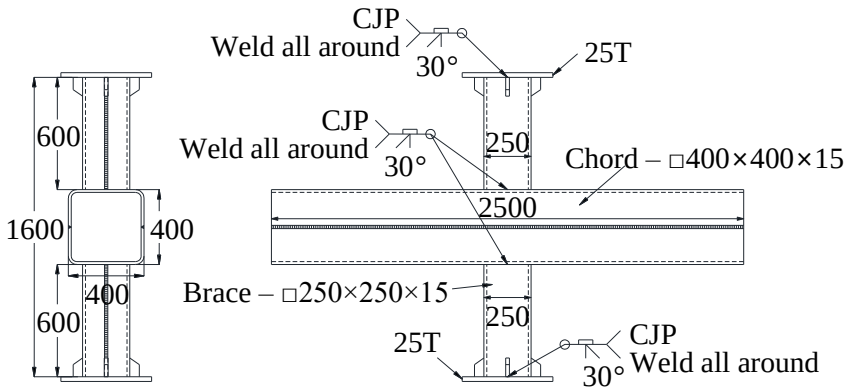

Figure 3.1 Drawing of the geometry of specimen #1 and specimen #2

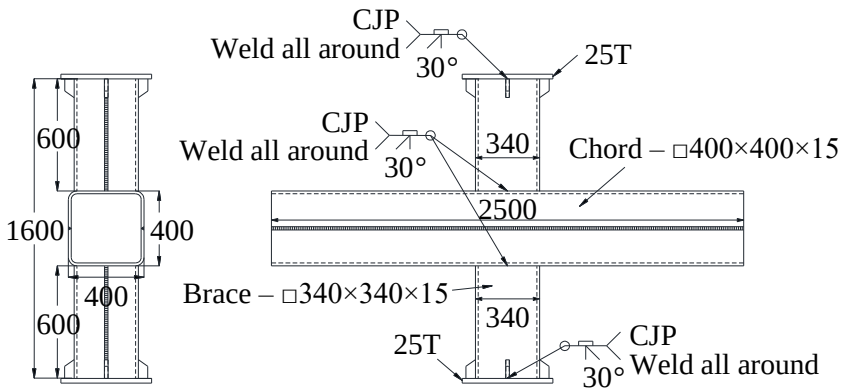

Figure 3.2 Drawing of the geometry of specimen #3 and specimen #4

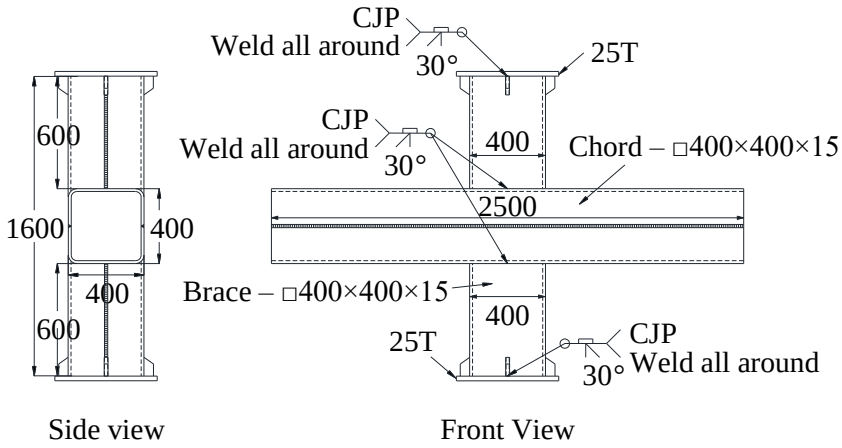

Figure 3.3 Drawing of the geometry of specimen #5 and specimen #6

The length of the braces was designed to spread out the load transferred from the braces. The length of the chord should be long enough to distribute stresses. The welded lines at the center of the chord section were positioned to investigate the negative effect of welded parts. The bearing plates with a thickness of 25 mm welded at the ends of the braces of specimens were fabricated from SM490.

3.2. Fabrication and test setup

3.2.1. Fabrication of specimens

The sections of the chord and the braces were 2-seam RHS assembled by two channel section. Figure 3.4 shows the drawing of the 2-seam RHS section. As shown in the Figure, two channel sections are welded using different weld rod depending on the steel applied to RHS. For the ordinary steel SM490, weld rod named K71T is used to weld two channel sections together. For HSA800 steel, weld rod PKW900 is used instead of K71T which is not be applicable to

weld high-strength steel because of the differences of ultimate strength between the steel and the weld rod. The ultimate stress of PKW900 is about 900 MPa which could be used for overmatching welding with HSA800 steels.

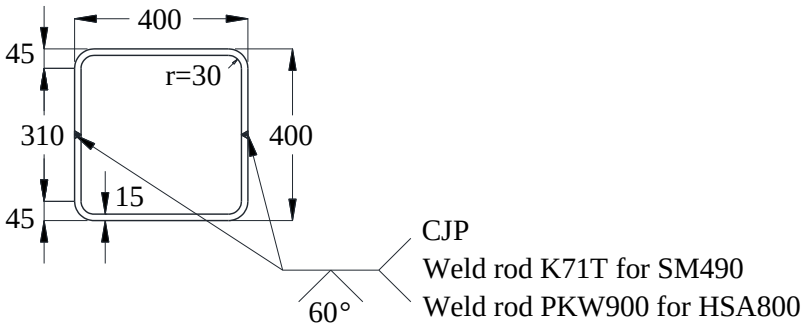

Figure 3.4 2-seam RHS section with a width and height of 400 mm

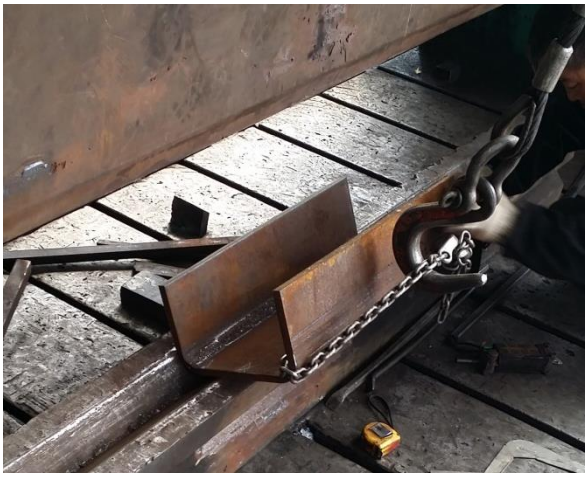

Figure 3.5 Bending procedure of channel sections (for brace section)

Channel sections to assemble chords and braces were bent by pressing machine with inner radius of 30mm. The press bending procedures of the channel sections for chord and braces are shown in Figure 3.5 and Figure 3.6. The plate is bent as the ram of the pressing machine moves downward to die.

Repeating this step for several times, the plate is formed to be a channel section.

Figure 3.6 Bending procedure of channel sections (for chord section)

3.2.2. Compression test setup

The axial compression tests of RHS X-joints were carried out by using a 10,000kN UTM (abbreviation of Universal Testing Machine). As shown in the Figure 3.7, UTM head was placed at the top surface of the specimen's bearing plate to apply a force.

Figure 3.7 Test setup of RHS X-joints under axial compression

3.3. Test results

3.3.1. Material test results

The properties of steels applied on the specimens were measured by tensile tests. A total of six tensile test coupons were cut out from two plates before manufacture process of the specimens. Three test coupons were obtained from the plate made up of ordinary steel SM490 while the others were cut out from the plate consisted of HSA800. Figure 3.8 shows six stress-strain curves measured from tensile tests of steels. The stress-strain curves shown as solid lines were obtained from the tensile test results of ordinary steel and dotted

lines represent the stress-strain relations of high-strength steel

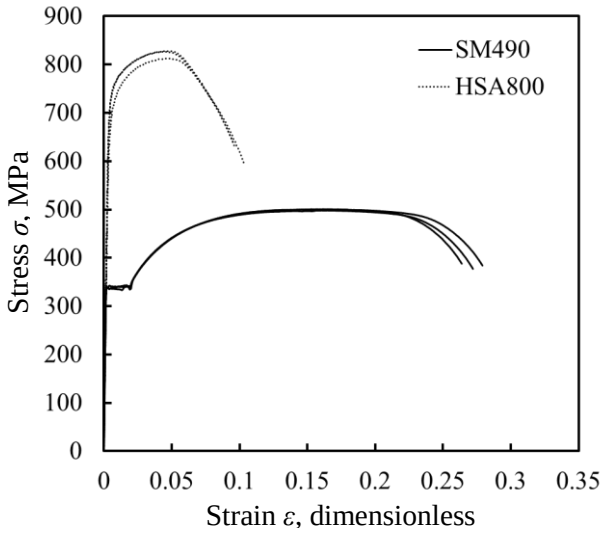

Figure 3.8 Stress-strain relations measured from tensile tests of steels (SM490 and HSA800)

The stress-strain relations of ordinary steels show clear yield plateau which could absorb energy without increment of stress. Strain hardening was observed from the strain over 0.018 (1.8%) until the test specimens were fractured at about the strain of 0.1 (10%). Otherwise, the tested coupons of high-strength steel gradually lost its stiffness before reaching at the peak of stress. Moreover, while ordinary steels could undergo more deformations after the peak stress, the stress of the specimens fabricated from high-strength steel rapidly decrease. The areas enclosed by the stress-strain curves, representing the energy absorbed by the material, of HSA800 specimens were clearly smaller than those of SM490.

Table 3.2 shows the material properties of steels measured from test results. The yield stresses reported in the Table were determined by 0.2%

offset method.

Table 3.2 Summary of tensile test results

Steel	Elastic modulus, MPa	Measured yield stress, MPa	Measured tensile stress, MPa	Measured yield ratio (σ_y/σ_u)	Yield strain ε_y, %
SM490 (15T)	236828	338	501	0.67	0.150
	232580	336	500	0.67	0.156
	224135	341	498	0.68	0.214
HSA800 (15T)	228184	729	827	0.88	0.500
	222909	737	827	0.89	0.570
	218748	680	812	0.84	0.570

*NOTE: Nominal yield stress and tensile stress of the steels
i. SM490: $\sigma_{y,n}$ = 325 MPa / $\sigma_{u,n}$ = 490 MPa
ii.HSA800: $\sigma_{y,n}$ = 650 MPa / $\sigma_{u,n}$ = 800 MPa

3.3.2. Test results of specimens with β = 0.625

i. X90–325–0.625–26.7

Figure 3.9 Chord plastification (X90–325–0.625–26.7)

As shown in Figure 3.9, chord plastification was observed from β = 0.625 specimen with SM490. The calculated nominal strength was 751 kN and the experimental strength was determined by 3% indentation criteria (Lu et al. 1994).

ii. X90–650–0.625–26.7

For β = 0.625 specimen of HSA800 also shows chord plastification behavior at relatively small indentation. The specimen with HSA800 failed much earlier than SM490 specimen, due to fracture (see Figure 3.10) at deformation about 10% of b_0. Despite of fracture occurred due to the low ductility of the chord face fabricated from HSA800, the experimental strength was 1270 kN which exceeds EC3 nominal strength about 30%.

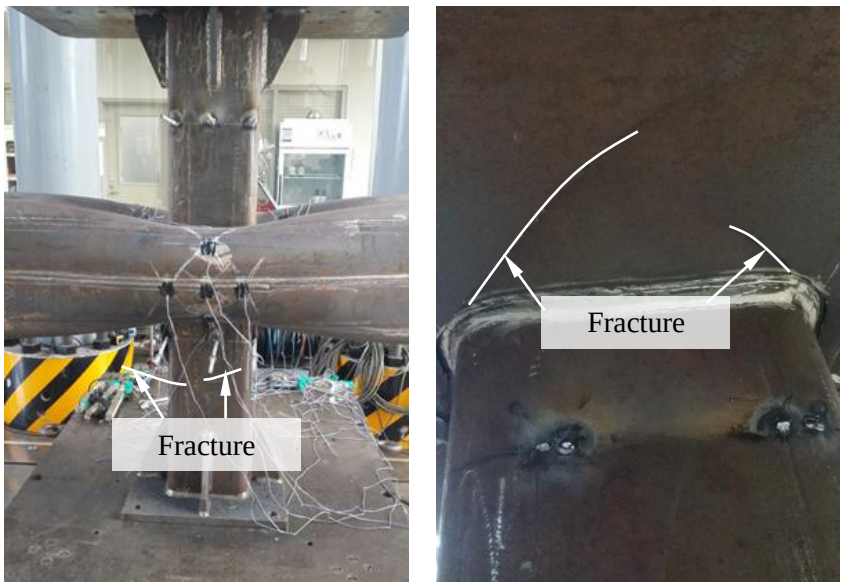

Inner view of the chord Lower face of the chord

Figure 3.10 Fracture occurred at the chord lower face (X90–650–0.625–26.7)

iii. Comparison of test results of two specimens

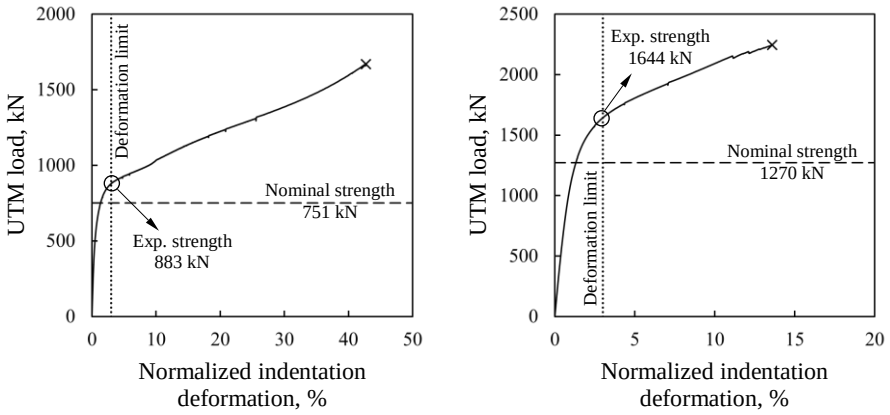

Figure 3.11 Experimental load–indentation curves of β = 0.625 specimens fabricated from SM490 (left) and HSA800 (right)

Figure 3.11 shows the load-indentation curves. Graph on the left shows the P-Δ curve of specimen X90–325–0.625–26.7 and graph on the right shows the P-Δ curve of specimen X90–650–0.625–26.7. Table 3.3 shows the results of the test specimens with β = 0.625.

Table 3.3 Test results summary (specimens with β = 0.625)

Specimen	**Measured yield stress f_y, MPa**	**EC3 nominal strength N_{EC3}, kN**	**Experimental strength N_{exp}, kN**	**N_{exp}/N_{EC3}, %**
X90–325 –0.625–26.7	388	751	880	118
X90–650 –0.625–26.7	715	1270 (1587)†	1644	129 (104)‡

† Without applying strength reduction factor
‡ Strength ratio without applying strength reduction factor

As shown in Table 3.3, the experimental strengths of the specimens with β = 0.625 were 118% (SM490) and 129% (HSA800) of EC3 nominal strength

according to 3% indentation criteria. Note that the unreduced EC3 nominal strength of X90–650–0.625–26.7 (HSA800) is very close to the experimental strength (just 4% difference).

3.3.3. Test results of specimens with β = 0.850

i. X90–325–0.850–26.7

Figure 3.12 Bulging occurred at the mid-height of the chord sidewall (X90–325–0.850–26.7)

As shown in Figure 3.12, a bulging occurred at the mid-height of the chord sidewall. It seems that the specimen failed by the mixed failure mode of chord plastification and chord sidewall buckling. The measured strength of the specimen was 2257 kN which exceeds EC3 nominal strength of 1649 kN. However, the peak strength of this specimen was observed at 1% of indentation deformation, the experimental strength was determined by the peak strength. It was clearly verified that the behavior of RHS X-joints

depends on the value of β.

ii. X90–650–0.850–26.7

A bulging was observed as occurred in specimen X90–325–0.850–26.7. The failure mode of this specimen seems to be identical with the other specimen fabricated from SM490. EC3 nominal strength calculated by chord plastification strength equation was 2788kN while the experimental strength determined by the peak value of the load-indentation graph was 4003 kN.

Figure 3.13 Bulging occurred at the mid-height of the chord sidewall (X90–650–0.850–26.7)

iii. Strength comparison

The relations between experimental strengths and the indentation deformation measured in compression test of RHS X-joints β = 0.85 were shown as the following graphs. The graph on the left side shows the P-Δ relationship of

specimen fabricated from ordinary steel (SM490) and the other shows the *P*-Δ of the test specimen fabricated from high-strength steel (HSA800).

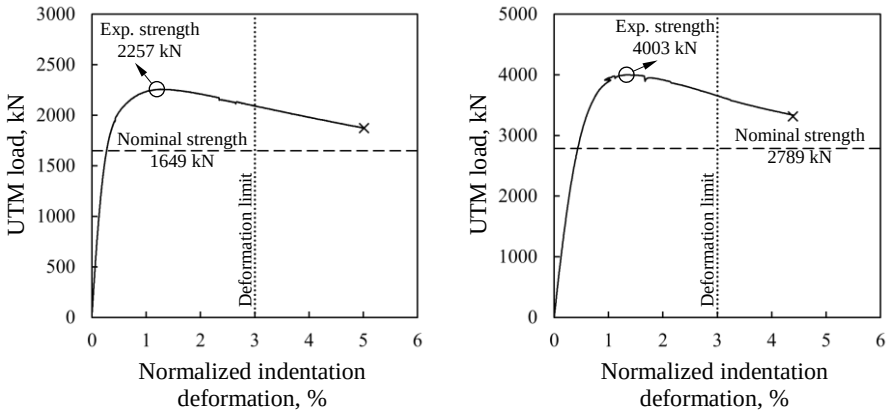

Figure 3.14 Experimental load–indentation curves of β = 0.85 specimens fabricated from SM490 (left) and HSA800 (right)

Table 3.4 shows the results of the test specimens with β = 0.850. The experimental strengths of two specimens with β = 0.85 were 137% (SM490) and 144% (HSA800) of EC3 nominal strengths, implying the conservatism in current EC3. Even without applying the strength reduction factor 0.8, the experimental strength of HSA800 specimen was higher than EC3 nominal strength by about 15%.

Table 3.4 Test results summary (specimens with β = 0.850)

Specimen	**Measured yield stress f_y, MPa**	**EC3 nominal strength N_{EC3}, kN**	**Experimental strength N_{exp}, kN**	**N_{exp}/N_{EC3}, %**
X90–325 –0.850–26.7	388	1647	2257	137
X90–650 –0.850–26.7	715	2788 (3485)†	4003	144 (115)‡

† Without applying strength reduction factor
‡ Strength ratio without applying strength reduction factor

3.3.4. Test results of specimens with β = 1.0

i. X90–325–1.000–26.7

The sidewalls of X90–325–1.000–26.7 deformed inward from their original positions while the other specimens show the bulging at the center of the chord sidewalls. Figure 3.15 shows the buckled shapes of the chord sidewalls. The experimental strength of specimen X90–325–1.000–26.7 determined by the peak value obtained from the P-Δ curve was 4553 kN while the strength predicted by EC3 was only 1860 kN. EC3 clearly gives a conservative prediction to β = 1 RHS X-joints.

Figure 3.15 The chord sidewall indented at the mid-height of the specimen (X90–325–1.000–26.7)

ii. X90–650–1.000–26.7

The sidewalls of X90–650–1.000–26.7 deformed inward and outward from their original positions. The buckled shapes of the chord sidewalls were

shown in the following photos. EC3 nominal strength was calculated as the value of 1845 kN which severely underestimate the experimental strength of this specimen determined by the peak strength of 8895 kN.

Figure 3.16 The chord sidewall buckled inward and outward (X90–650–1.000–26.7)

iii. Strength comparison

The experimental results are compared in this paragraph. Figure 3.17 shows the load-deformation relationships of specimens with β = 1 while Table 3.5 shows the summary of the test results.

The experimental strengths normalized by EC3 nominal strengths were respectively 245% for X90–325–1.000–26.7 (SM490) and 482% for X90–650–1.000–26.7 (HSA800), clearly indicating that current EC3 strength formula for chord sidewall buckling limit state is unacceptably conservative and should be improved.

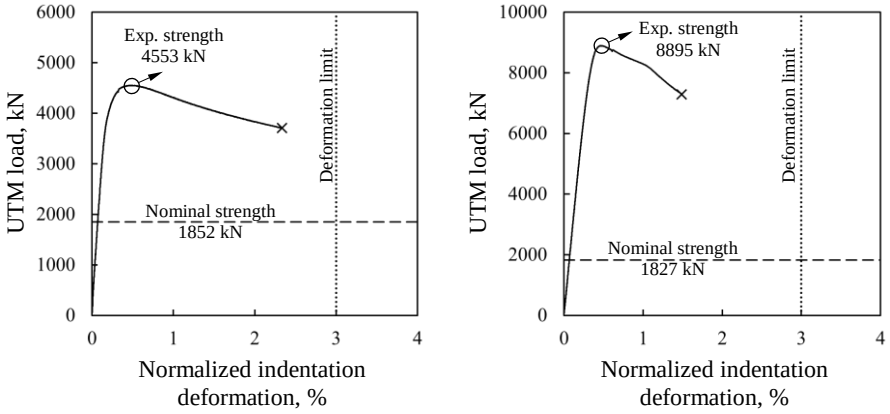

Figure 3.17 Experimental load–indentation curves of β = 1.0 specimens fabricated from SM490 (left) and HSA800 (right)

Table 3.5 Test results summary (specimens with β = 1.000)

Specimen	**Measured yield stress f_y, MPa**	**EC3 nominal strength N_{EC3}, kN**	**Experimental strength N_{exp}, kN**	**N_{exp}/N_{EC3}, %**
X90–325 –0.850–26.7	388	1860	4553	245
X90–650 –0.850–26.7	715	1845 (2307)†	8895	482 (386)‡

† Without applying strength reduction factor
‡ Strength ratio without applying strength reduction factor

3.3.5. Load-deflection characteristics

In this article, the graphs representing normalized load-deflection relationships are shown to investigate the behavior of RHS X-joints with identical geometric and different grades of steels.

As can be seen in the left curve of Figure 3.18, the specimen with HSA800 failed much earlier than SM490 specimen due to the fracture of the chord lower face occurred at 10% normalized indentation deformation. On the

other hand, the specimens with β = 0.625 exceed the 3% ultimate deformation limit. While the specimen with ordinary steel could undergo more deformations without losing its strength, it seems that the specimen fabricated from high-strength steel (HSA800) also has enough ductility to resist deformations.

On the other hand, as shown in the right curve of Figure 3.18, the specimens with β = 0.625 show an almost identical behavior. The peak strength of the two specimens with β = 0.85 was reached at about 1% indentation. These joints are much more stiff and brittle than those with β = 0.625.

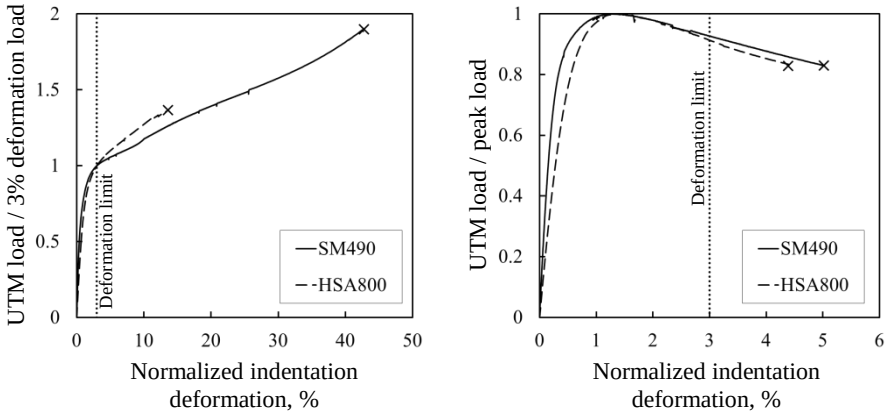

Figure 3.18 Normalized experimental load–indentation curves: specimens with β = 0.625 (left) and β = 0.850 (right)

Figure 3.19 shows the normalized experimental load versus normalized indentation deformation curve obtained from the experimental test of β = 1 specimens. As shown in right graph of Figure 3.18, the behaviors of these specimens are almost identical to each other. The peak strengths of these two specimens were reached at about 0.5% indentation deformation. The stiffest

and brittlest behaviors among the experimental tests were observed from these two specimens.

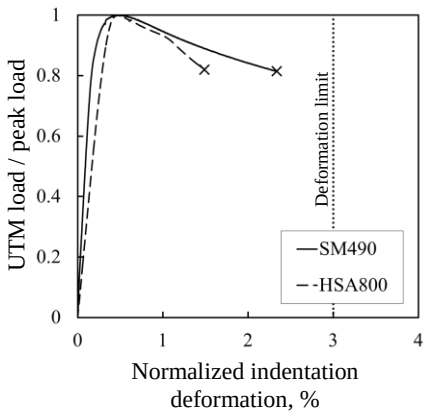

Figure 3.19 Normalized experimental load–indentation curve: specimens with β = 1.00

3.4. Comparative analysis of RHS X-joints with β = 1

After collecting test data available in the literature as shown in section 2.4 and this experimental program, a comparison was tried in this section with Eurocode3 (2005) and AISC (2010) formula and that suggested by Becque and Cheng (2016).

3.4.1. Sidewall buckling strength equation in Eurocode3 (2005)

To evaluate the sidewall buckling strength formula of Eurocode3 (2005), test data was collected from available literatures and the buckling strengths were normalized by yield strength equation suggested in Wardenier (1982). The normalized strengths (N_b/N_y) were fitted on “c” curve of Eurocode3 (2005)

multiple column curves. Figure 3.11 shows the relation between the buckling reduction factor χ and the normalized slenderness ratio $\overline{\lambda}$.

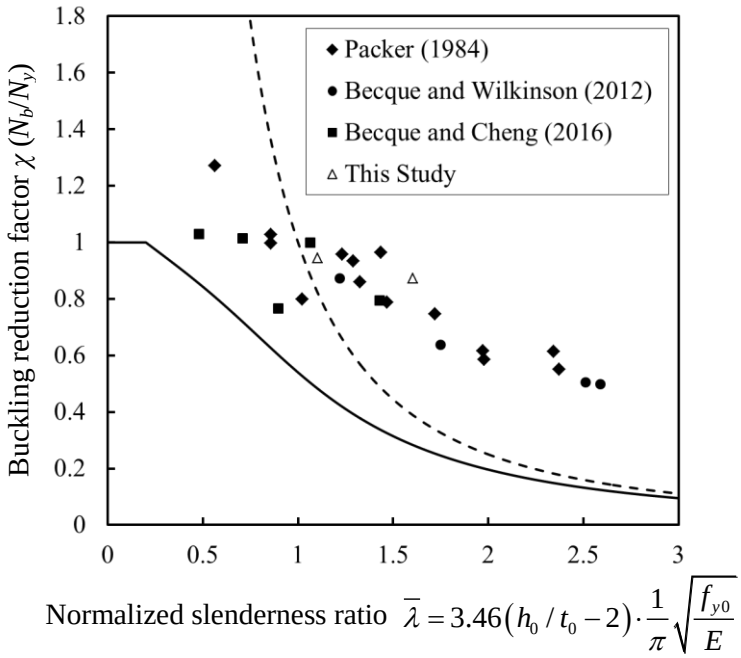

Figure 3.20 Comparison between β = 1 RHS X-joints experimental strengths normalized by EC3 chord sidewall buckling strength

The solid line and the dotted line in Figure 3.20 represent the multiple curve "c" of Eurocode3 (2005) multiple column curves and the elastic column buckling curve, respectively.

Table 3.6 Comparative analysis of EC3 chord sidewall buckling equation

N_{exp} / N_b	Maximum	minimum	Mean	MSE	COV
	6.25	1.50	3.81	3.32	0.87

The statistic parameters were calculated for the evaluation purpose as shown in Table 3.6. Mean square error (MSE) was calculated by equation 3.1:

$$\mathrm{MSE} = \frac{1}{n}\sum_{i=1}^{n}\left(y_i - \tilde{y}_i\right)^2 \tag{3.1}$$

where y_i is the normalized experimental strength and $\tilde{y}_i$ is the true value. When the experimental strength is equal to the strength determined by EC3 sidewall buckling equation, y_i is equal to unity. Therefore, in this comparison, the true value $\tilde{y}_i$ is set as a unity.

The maximum value and the mean value of the normalized experimental strengths were 6.25 and 3.44 respectively, which imply that EC3 sidewall buckling strength gives extremely conservative predictions. Even the minimum value was 1.50; this formula still underestimates the actual strength. Moreover, a large scatter indicated by the high coefficient of variation (COV=0.81). From these parameters calculated here, it is obvious that EC3 sidewall buckling strength equation needs to improve.

3.4.2. Web crippling strength suggested in AISC (2010)

As mentioned in the article 2.1.3, AISC (2010) suggest to determine the strength of X-joints with β = 1 by the chord yield strength and the RHS web crippling strength. The minimum value between these strengths becomes the strength of β = 1 RHS X-joints.

Therefore, in Figure 3.21, the data plotted as black squares represents the experimental strength normalized by the chord sidewall yielding strength while the data plotted as the symbol × represents the experimental strength normalized by the web crippling strength. The strengths of X-joints with relatively heavy sections (with low h_0-t_0 ratio) were mostly determined by chord yielding strength while joints with light sections were governed by web

crippling behavior.

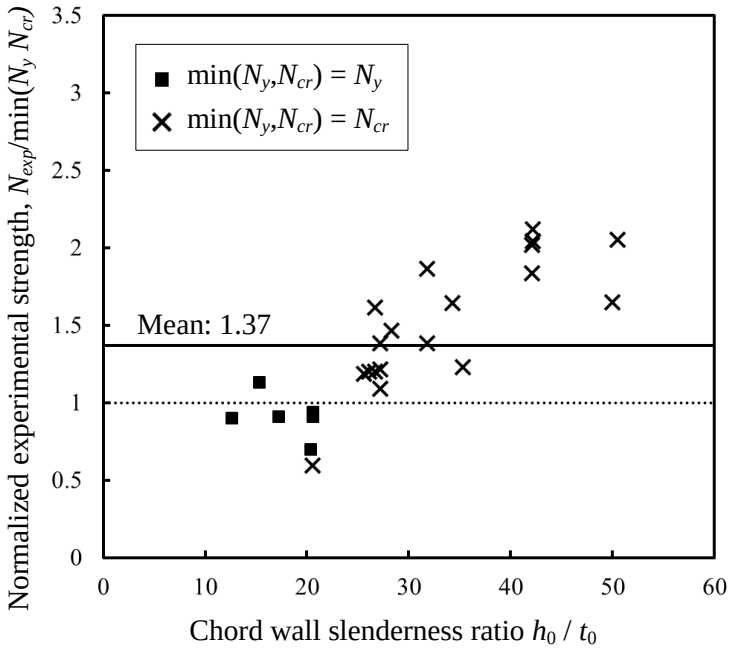

Figure 3.21 Comparison between β = 1 RHS X-joints experimental strengths normalized by AISC β = 1 RHS X-joints strength

The maximum value and the mean value of the normalized experimental strengths were 2.12 and 0.59 respectively. The accuracy of the prediction was better than that of EC3 strength equation; however, it was not sufficient enough. Furthermore, actual strengths of several specimens were overestimated by the web crippling strength equation. COV for this comparison was 0.42 which is greater value than that of EC3 (see Table 3.7). As a consequence, the formula suggested in AISC (2010) gives the normalized strength closer to value of unity than that of EC3, but it often gives a unsafe prediction which means that this method is not appropriate to use as a strength formula in structural codes.

Table 3.7 Comparative analysis of AISC (2010) RHS X-joints strength with β = 1

N_{exp} / N_b	Maximum	minimum	Mean	MSE	COV
	2.12	0.59	1.36	0.57	0.42

3.4.3. Sidewall buckling strength equation proposed by Becque and Cheng (2016)

The experimental strengths were evaluated by the equation suggested in Becque and Cheng (2016).

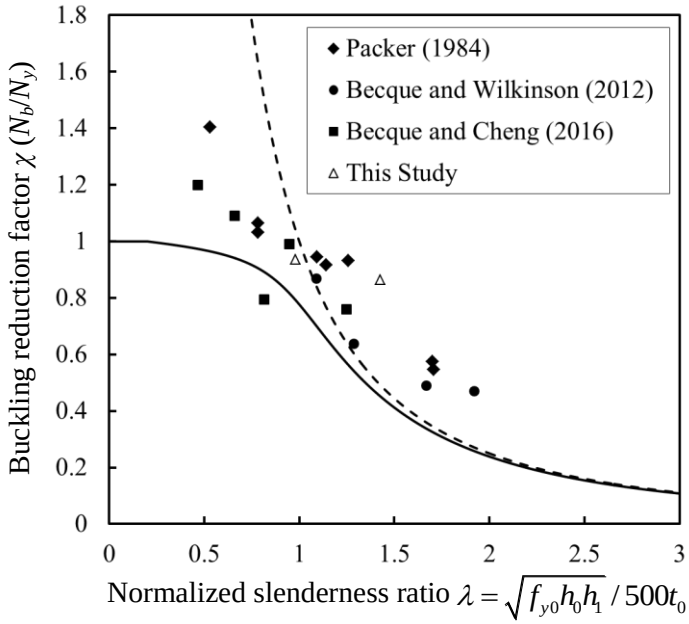

Figure 3.22 Comparison between β = 1 RHS X-joints experimental strengths normalized by strength equation of Becque and Cheng (2016)

The maximum value and the mean value of the normalized experimental strengths were 1.91 and 0.89 respectively. The accuracy of the prediction was the best among the current design strengths. However, quite high value of COV (= 0.34) was observed for this method which shows the large deviation

of prediction of strengths. The statistical parameters calculated in this article are shown in Table 3.8.

Table 3.8 Comparative analysis of the strength for RHS X-joints with β = 1 suggested in Becque and Cheng (2016)

N_{exp} / N_b	Maximum	minimum	Mean	MSE	COV
	1.91	0.89	1.39	0.48	0.34

3.5. Summary

A total of six RHS X-joint specimens were tested under compression with β values and grades of steel as the key test variables. The results can be summarized as follows.

1. The experimental strengths of the high-strength RHS X-joint specimens with β = 0.625 and β = 0.850 was more reasonably but still conservatively predicted by the EC3 chord plastification equation when the strength reduction factor 0.8 was neglected.
2. As β value becomes higher beyond 0.6, the joint strength is determined by the peak strength criteria, not by the 3% indentation criteria, and the joint becomes less ductile.
3. For the case of β = 1.00, the test results of this study clearly showed that current sidewall buckling strength equations have an insufficient accuracy and should be improved based on different strength formulation.

Chapter 4

New Design Formula for Sidewall Buckling

4.1. Introduction

As mentioned in previous chapters, CIDECT (2009) and Eurocode3 (2005) are based on the column model suggested by Wardenier (1982), and AISC (2010) is based on the plate buckling model derived in the work of Chen and Newlin (1971). However, nominal strengths of RHS X-joints with equal-width evaluated by the representative design standards are too conservative and inaccurate. To evaluate the actual strengths of RHS X-joints with β = 1 more accurately, Becque and Cheng (2016) suggested alternative design equation but it needs to be improved for more consistency and accuracy. Therefore, in this chapter, the new design equation for β = 1 RHS X-joints will be derived based on the theoretical model of plate buckling.

To derive an accurate sidewall buckling equation, the elastic buckling strength and the yield strength of equal-width RHS X-joints should be defined

as exactly as possible.

In section 4.2, a theoretical model based on plate buckling is established and the elastic buckling stress was derived by the principle of stationary total potential energy obtained from the assumed shape function.

Section 4.3 shows the conditions assumed in section 4.2 were numerically validated with the ABAQUS finite element analysis models. .

Finally, section 4.4 gives a proposal of new sidewall buckling strength formula. The derivations of the new slenderness ratio and the inelastic sidewall buckling strength equation will be introduced and the comparative analysis results will be described in this section.

4.2. Theoretical model: elastic plate buckling model

4.2.1. Basic assumptions

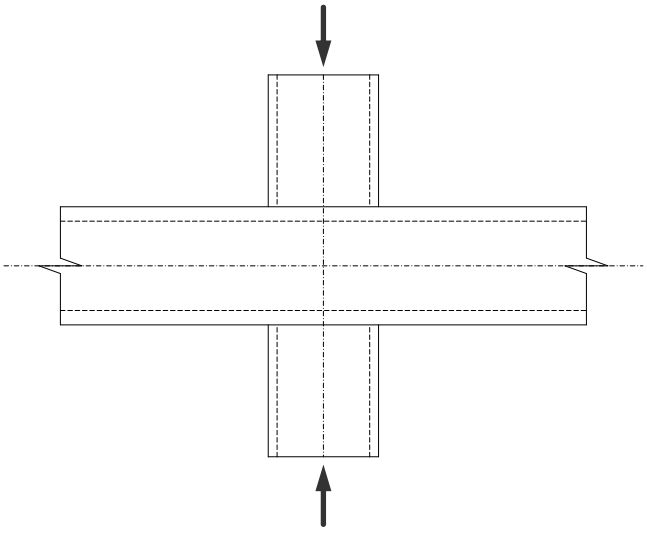

Figure 4.1 General RHS β = 1 X-joints

A theoretical model was developed by Becque and Cheng (2016) representing the chord sidewall by a plate with thickness t_0, which extends to infinity on both sides, as can be seen in Figure 4.2.

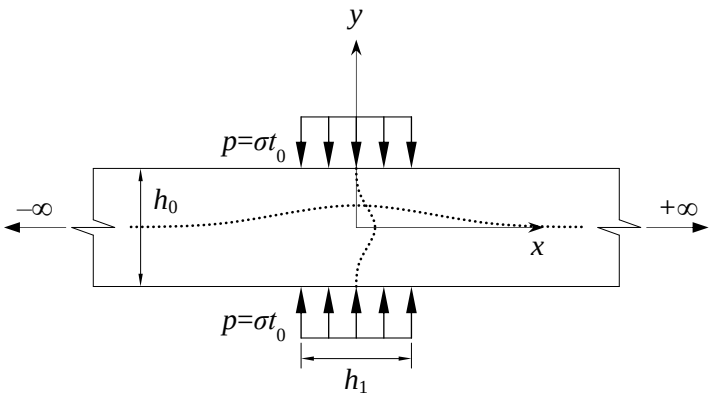

Figure 4.2 Theoretical model of β = 1 RHS X-joints based on plate buckling

The load p transferred from the brace sidewall into the chord sidewall is uniformly distributed over the brace width h_1. The total load N carried by the connection (comprising two sidewalls) is then given by:

$$N = 2ph_1 = 2\sigma t_0 h_1 \tag{4.1}$$

Even though the actual boundary conditions of the edges supported by the braces are not exactly same as the clamped supported condition, for the simplicity of the buckling stress equation and the flexural rigidity of the braces supporting the edges to behave rigidly, a fixed supported condition is assumed to the transverse edges while the edges are assumed to be simply supported in Becque and Cheng (2016).

For the longitudinal direction, as assumed in the work of Becque and Cheng (2016), the exponential Gauss function is chosen to represent the

buckling shaped. This function is an ideal candidate to capture the localized nature of the failure mode, since its ordinates approach zero almost immediately when leaving a localized area around the origin.

4.2.2. Composition of buckled shape function

The buckled shape of the sidewalls could be expressed as in the following equation:

$$w(x,y) = \Delta w_x(x) w_y(y) \tag{4.2}$$

where w is the shape function of the buckled plate, w_x is the x-direction (longitudinal direction of the chord) components of the shape function, and w_y is the y-direction (transverse direction of the chord) components of the shape function. Equation 4.2 representing the buckled shape function as a multiplied form of two functions with different variables, is based on the concept regarding the buckled shape of the plate behaves independently with the directions transverse to each other.

Therefore, the proposed deformed shape is expressed by the following function:

$$w(x,y) = \Delta w_x w_y = \Delta \cdot e^{-x^2/2s^2} \cdot \frac{1}{2}\left[1+\cos\left(2\pi\frac{y}{h_0}\right)\right] \tag{4.3}$$

where h_0 is the height of the chord, s is the parameter in length dimension having mathematical meaning of the standard deviation, and Δ is the amplitude of the buckled shape.

The variables x and y are in the range of $(-\infty, \infty)$ and $[-h_0/2, h_0/2]$

respectively. Figure 4.3 shows the assumed buckling shape function in general view and the buckled shape in top view is shown in Figure 4.4.

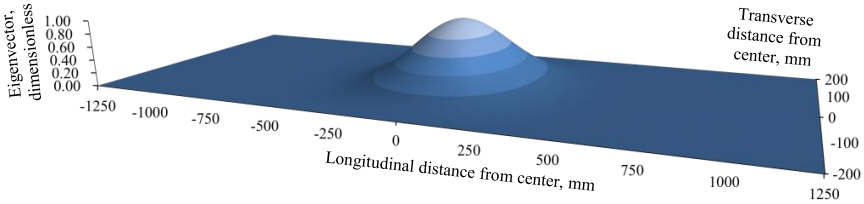

Figure 4.3 Assumed buckling shape function (general view)

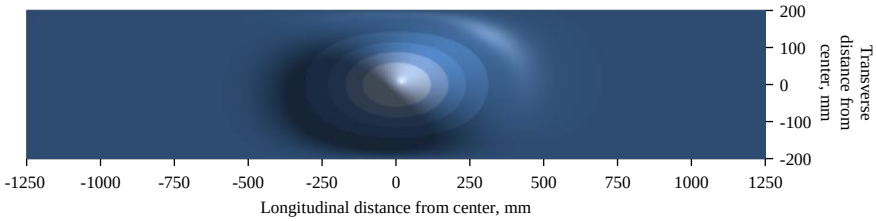

Figure 4.4 Assumed buckling shape function (top view)

4.2.3. Calculation of total potential energy of buckled plate

Timoshenko and Gere (1961) introduce the equation of strain energy in bending of plates. The strain energy U could be expressed as the following equation:

$$U = \frac{D}{2}\int_{-\infty}^{\infty}\int_{-h_0/2}^{h_0/2}\left[\left(\frac{\partial^2 w}{\partial x^2}\right)^2 + \left(\frac{\partial^2 w}{\partial y^2}\right)^2 + 2\nu\left(\frac{\partial^2 w}{\partial x^2}\right)\left(\frac{\partial^2 w}{\partial y^2}\right) + 2(1-\nu)\left(\frac{\partial^2 w}{\partial x \partial y}\right)^2\right]\mathrm{d}y\mathrm{d}x \tag{4.4}$$

where w is a deformed shape of a plate, and D is the flexural rigidity of the plate given by:

$$D = \frac{Et_0^3}{12(1-\nu^2)} \tag{4.5}$$

where E is the elastic modulus of the plate, t_0 is the thickness of the chord. This equation is derived in the case of bending of a plate submitted to the simultaneous action of transverse loads and of forces applied in the middle plane of the plate. Substituting the buckled shape function to this equation eventually leads to the following equation:

$$U = \sqrt{\pi}\Delta^2 D \cdot \frac{1}{s^2} \times \left[\left(\frac{9}{64} \cdot \frac{h_0}{s} \right) + \left(\pi^4 \cdot \frac{s^3}{h_0^3} \right) + \left(\frac{\pi^2}{4} \cdot \frac{s}{h_0} \right) \right] \tag{4.6}$$

The potential energy V of the applied stresses is given by:

$$V = -\frac{\sigma t_0}{2} \int_{-h_1/2}^{h_1/2} \int_{-h_0/2}^{h_0/2} \left(\frac{\partial w}{\partial y} \right)^2 \mathrm{d}y\mathrm{d}x \tag{4.7}$$

where σ is the uniformly distributed stress applied on the chord. Using the shape function of the buckled plate, the equation of the potential energy yields to:

$$V = -\frac{\pi^2 \sqrt{\pi}}{4} \Delta^2 \sigma t_0 \frac{s}{h_0} \cdot \mathrm{erf}\left(\frac{h_1}{2s} \right) \tag{4.8}$$

where erf is the error function (also called the Gauss error function) defined as:

$$\mathrm{erf}\left(x\right) \equiv \frac{1}{\sqrt{\pi}} \int_{-x}^{x} e^{-t^2} \mathrm{d}t = \frac{2}{\sqrt{\pi}} \int_{0}^{x} e^{-t^2} \mathrm{d}t \tag{4.9}$$

4.2.4. Buckling stress calculation by the energy principle

By the principle of stationary total potential energy, the derivatives of the total energy ($U + V$) with respect to B and Δ are set equal to zero:

$$\frac{\partial(U+V)}{\partial\Delta}=0 \quad \text{and} \quad \frac{\partial(U+V)}{\partial s}=0 \tag{4.10}$$

i. $\dfrac{\partial(U+V)}{\partial\Delta}=0$

Substituting equation 4.6 and equation 4.8 into the equation above, the relationship between two unknowns were obtained as the followings:

$$2\sqrt{\pi}\Delta D\frac{h_0}{s^3}\times\left[\frac{9}{64}+\pi^4\left(\frac{s}{h_0}\right)^4+\frac{\pi^2}{4}\left(\frac{s}{h_0}\right)^2\right]-\frac{\pi^2\sqrt{\pi}}{2}\Delta\sigma t_0\frac{s}{h_0}\cdot\operatorname{erf}\left(\frac{h_1}{2s}\right)=0$$

If $\Delta = 0$, the shape function for the buckled plate $w = 0$. This condition yields w to trivial solution. Therefore, the equation $\dfrac{\partial(U+V)}{\partial\Delta}=0$ with $\Delta\neq 0$ yields to the following equations:

$$\sigma_{cr}=\frac{1}{\pi^2}\frac{D}{t_0h_0^2}\times\frac{\dfrac{9}{16}\left(\dfrac{h_0}{s}\right)^4+\pi^2\left(\dfrac{h_0}{s}\right)^2+4\pi^4}{\operatorname{erf}\left(\dfrac{h_1}{2s}\right)} \tag{4.11}$$

ii. $\dfrac{\partial(U+V)}{\partial s}=0$

As similar to the previous derivation, substituting energy equation U and V (equation 4.6 and 4.8, respectively) to $\dfrac{\partial(U+V)}{\partial s}=0$ yields the equation to:

$$\frac{\sqrt{\pi}\Delta^2D}{4}\frac{h_0}{s^4}\times\left[4\pi^4\cdot\frac{s^4}{h_0^4}-\pi^2\cdot\frac{s^2}{h_0^2}-\frac{27}{16}\right]-\frac{\pi^2\sqrt{\pi}}{4}\Delta^2\sigma\frac{t_0}{h_0}\frac{\partial\left(s\cdot\operatorname{erf}\left(h_1/2s\right)\right)}{\partial s}$$

$$=\frac{\sqrt{\pi}\Delta^2D}{4}\frac{h_0}{s^4}\times\left[4\pi^4\cdot\frac{s^4}{h_0^4}-\pi^2\cdot\frac{s^2}{h_0^2}-\frac{27}{16}\right]-\frac{\pi^2\sqrt{\pi}}{4}\Delta^2\sigma\frac{t_0}{h_0}\left[\operatorname{erf}\left(\frac{h_1}{2s}\right)-\frac{h_1e^{-\frac{h_1^2}{4s^2}}}{s\sqrt{\pi}}\right]=0 \tag{4.12}$$

If $\Delta = 0$, the shape function for the buckled plate $w = 0$. This condition yields w to trivial solution. Therefore, the critical stress term σ_{cr} is derived as the following equation:

$$\sigma_{cr} = \frac{1}{\pi^2}\frac{D}{t_0 h_0^2} \times \frac{\frac{27}{16}\left(\frac{h_0}{s}\right)^4 + \pi^2\left(\frac{h_0}{s}\right)^2 - 4\pi^4}{\frac{h_1}{s\sqrt{\pi}}e^{-h_1^2/4s^2} - \operatorname{erf}\left(\frac{h_1}{2s}\right)} \tag{4.13}$$

Equation 4.11 and equation 4.13 represent the identical term, the critical stress σ_{cr}. Therefore, let right sides of these equations are equal to each other; the equation to obtain the parameter s could be derived as:

$$\frac{1}{\pi^2}\frac{D}{t_0 h_0^2} \times \frac{\frac{9}{16}\left(\frac{h_0}{s}\right)^4 + \pi^2\left(\frac{h_0}{s}\right)^2 + 4\pi^4}{\operatorname{erf}\left(\frac{h_1}{2s}\right)} = \frac{1}{\pi^2}\frac{D}{h_0^2 t_0} \times \frac{\frac{27}{16}\left(\frac{h_0}{s}\right)^4 + \pi^2\left(\frac{h_0}{s}\right)^2 - 4\pi^4}{\frac{h_1}{s\sqrt{\pi}}e^{-h_1^2/4s^2} - \operatorname{erf}\left(\frac{h_1}{2s}\right)}$$

$$\Rightarrow \frac{9\left(\frac{h_0}{s}\right)^4 + 16\pi^2\left(\frac{h_0}{s}\right)^2 + 64\pi^4}{\operatorname{erf}\left(\frac{h_1}{2s}\right)} = \frac{27\left(\frac{h_0}{s}\right)^4 + 16\pi^2\left(\frac{h_0}{s}\right)^2 - 64\pi^4}{\frac{h_1}{s\sqrt{\pi}}e^{-h_1^2/4s^2} - \operatorname{erf}\left(\frac{h_1}{2s}\right)} \tag{4.14}$$

Solution: General case

Let $h_1 = \alpha h_0$. Then the equation to obtain s value yields to:

$$\frac{9\left(\frac{h_0}{s}\right)^4 + 16\pi^2\left(\frac{h_0}{s}\right)^2 + 64\pi^4}{\operatorname{erf}\left(\frac{\alpha h_0}{2s}\right)} = \frac{27\left(\frac{h_0}{s}\right)^4 + 16\pi^2\left(\frac{h_0}{s}\right)^2 - 64\pi^4}{\frac{\alpha h_0}{s\sqrt{\pi}}e^{-\alpha^2 h_0^2/4s^2} - \operatorname{erf}\left(\frac{\alpha h_0}{2s}\right)} \tag{4.15}$$

Substituting c to h_0/s could simplify this equation as:

$$\frac{\alpha e^{-\alpha^2 c^2/4}}{\sqrt{\pi}\cdot \mathrm{erf}\left(\alpha c/2\right)} = \frac{36c^3 + 32\pi^2 c}{9c^4 + 16\pi^2 c^2 + 64\pi^4} \tag{4.16}$$

The plate buckling stress could be determined by the value of c (= h_0/s) and α. The equation for the plate buckling stress σ_{cr} is equal to:

$$\sigma_{cr} = k\pi^2 \frac{Et_0^3}{12\left(1-\nu^2\right)} \frac{1}{h_0^2 t_0} = k\frac{\pi^2 D}{h_0^2 t_0} \tag{4.17}$$

where k is a numerical factor given by:

$$k = \frac{\frac{9}{16\pi^4}\left(\frac{h_0}{s}\right)^4 + \frac{1}{\pi^2}\left(\frac{h_0}{s}\right)^2 + 4}{\mathrm{erf}\left(\frac{h_1}{2s}\right)} = \frac{\frac{9}{16\pi^4}\left(\frac{h_0}{s}\right)^4 + \frac{1}{\pi^2}\left(\frac{h_0}{s}\right)^2 + 4}{\mathrm{erf}\left(\frac{\alpha h_0}{2s}\right)}$$

This factor k reflects the influence of h_1/h_0 affecting elastic buckling stresses of the theoretical model of β = 1 RHS X-joints.

Buckling stress could be calculated by substituting the solutions of two variables, α and c, obtained from equation 4.16 to equation 4.17. Since there are two unknown variables s and α in the equation of k factor, equation 4.17 could be solved with one of the variables determined. MATLAB fsolve command was used to solve this system of equations. The values of α were chosen before solving this equation and then s values could be obtained. As a result, the relationship between h_0/h_1 (=1/α) and k are shown as the following Figure and Table. The source codes of this command are reported in appendix A.

Table 4.1 Analytical solution of k at definite h_0/h_1 values

$1/\alpha$ (h_0/h_1)	0.25	0.5	1	2	4
k (analytical)	4.126	4.401	5.241	7.565	13.140

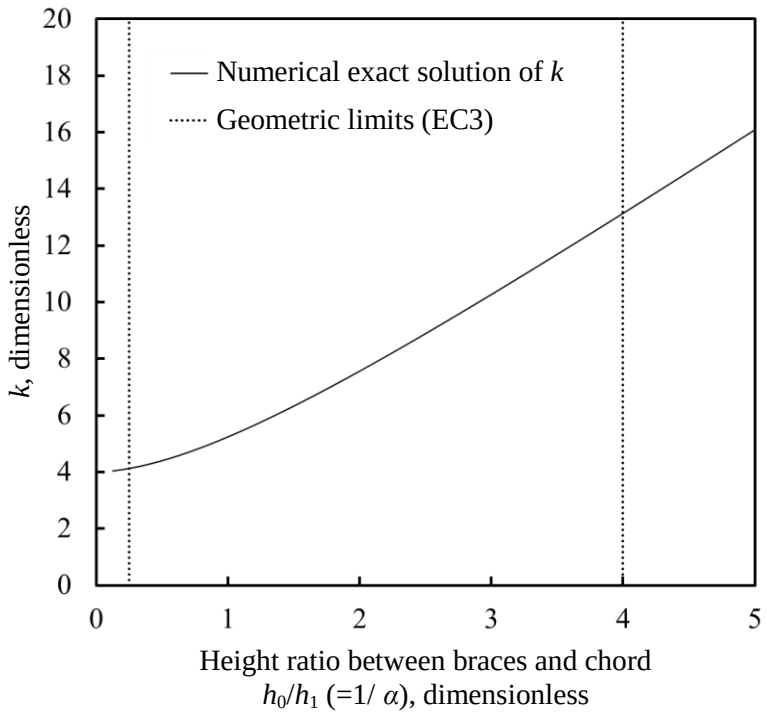

Figure 4.5 Relationship between k and h_0/h_1

By EC3 RHS X-joint geometric limitations, the ratio between the height and the width of the section should satisfy the following inequality:

$0.5 \le h_i / b_i \le 2$ (subscript i: 0 for a chord and n ($n \neq 0$) for a brace)

Since this is the buckling model of equal-width RHS X-joint, the width of the chord b_0 should be equal to the width of the braces b_1. Thus, aforementioned inequality limiting the height ratio between the chord and the brace could be modified as the following:

$$0.25 \le h_1 / h_0 \le 4 \tag{4.18}$$

where h_0 and h_1 are the height of the chord and the braces respectively.

To express the numerical exact solution of k by the simple equation, some functions were assumed and evaluated assessed with their simplicity and errors compared to the actual value of k in the range shown in equation 4.18. In Table 4.2, 1st, 2nd and 3rd order polynomials and the exponential function obtained from regression analysis were compared with the analytical k value.

Table 4.2 Comparison among approximated k values depending on $1/\alpha$ (h_0/h_1)

Height ratio between chord and brace $1/\alpha$ (=h_0/h_1), dimensionless		0.25	0.5	1	2	4
Numerical value of k, dimensionless		4.126	4.401	5.241	7.565	13.140
1st order polynomial	Equation	$2.186(h_0/h_1)+3.347$				
	Approximated k	3.894	4.440	5.533	7.719	12.091
	Error, %	5.62	0.89	5.57	2.04	7.98
2nd order polynomial	Equation	$0.288(h_0/h_1)^2+1.293(h_0/h_1)+3.718$				
	Approximated k	4.059	4.436	5.298	7.454	13.492
	Error, %	1.62	0.80	1.09	1.47	2.68
3rd order polynomial	Equation	$-0.08(h_0/h_1)^3+0.725(h_0/h_1)^2+0.710(h_0/h_1)+3.887$				
	Approximated k	4.109	4.413	5.240	7.547	13.048
	Error, %	0.41	0.27	0.02	0.24	0.70
Exponential form	Equation	$5.241 \cdot e^{0.32(h_0/h_1-1)}$				
	Approximated k	4.123	4.466	5.241	7.218	13.689
	Error, %	0.07	1.48	0.00	4.59	4.18

2nd and 3rd order polynomials are too complicated to use as approximated

solutions. Then 1st order polynomial and equation with exponential term could simply approximate the numerical solution of *k*. However, the accuracy of 1st order polynomial is not sufficient enough to describe *k* values (maximum 8% error occurs). Thus, the equation with exponential form is selected as an alternative. The exponential function is shown at Figure 4.6 compared with analytical solution *k* depending on h_0/h_1 value.

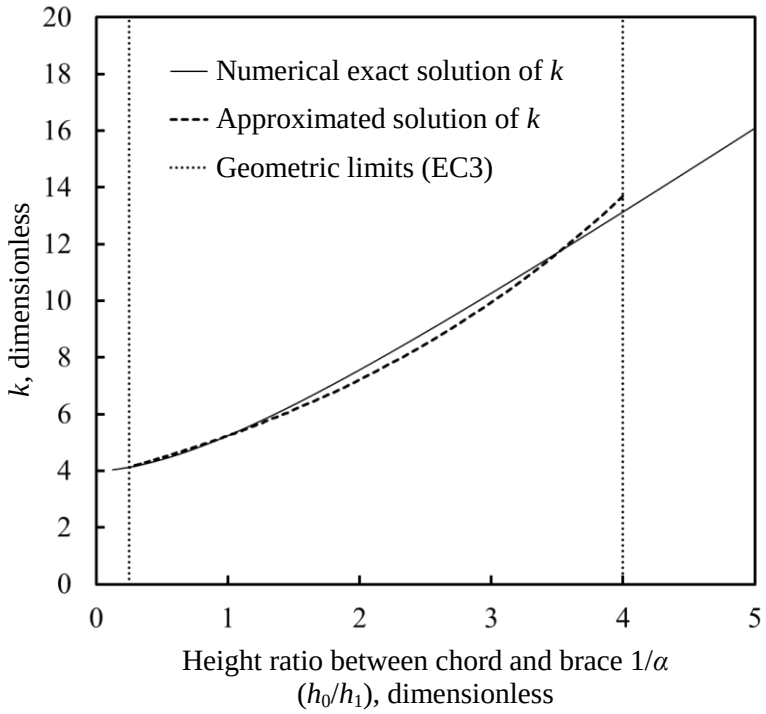

Figure 4.6 Analytical solution *k* and the approximated *k* depending on h_0/h_1

Substituting the approximated *k* function to equation 4.18, the elastic buckling strength equation could be obtained as shown in the equation below:

$$\sigma_{cr} = 5.2415 \cdot e^{0.32(h_0/h_1-1)} \cdot \frac{\pi^2 E}{12\left(1-\nu^2\right)} \frac{t_0^2}{h_0^2} \tag{4.19}$$

This buckling stress can be compared with the buckling strength suggested in the work done by Becque and Cheng (2016).

$$\sigma_{cr,Becque} = 1.346 \frac{\pi^2 E}{12\left(1-\nu^2\right)} \frac{t_0^2}{h_0 h_1} \tag{4.20}$$

As the equations shown above, the elastic stress derived in Becque and Cheng (2016) is inversely proportional to h_0 and h_1 and directly proportional to the square term of t_0. However in the proposed elastic buckling stress equation, the stress is not inversely proportional to h_1 value. Instead, the height ratio between the chord and the braces h_0/h_1 is included in exponential function.

For the case of $h_0 = h_1$, the exponential term yields to unity which has no influence to the value of elastic buckling stress. Then the equations yields to:

$$\sigma_{cr,Becque} = 1.346 \frac{\pi^2 E}{12\left(1-\nu^2\right)} \frac{t_0^2}{h_0^2} \text{ and } \sigma_{cr,proposed} = 5.2415 \frac{\pi^2 E}{12\left(1-\nu^2\right)} \frac{t_0^2}{h_0^2}$$

Therefore, the ratio between $\sigma_{cr,\text{proposed}} / \sigma_{cr,\text{Becque}}$ could be obtained as:

$$\therefore \sigma_{cr,proposed} / \sigma_{cr,Becque} = \frac{5.2415}{1.346} = 3.89$$

Since $\sigma_{cr,proposed}$ is derived by the assumption that the shape function transverse to the chord direction is fixed, the buckling stress of it is about four times of $\sigma_{cr,Becque}$ which is based on the simply supported condition assumption of the shape function whose direction is transverse to the chord.

4.3. Validation by numerical analysis

An investigation of validity of the assumptions suggested in previous section will be discussed in the following section. In the first article of this section, finite element analysis models will be established and their validities are proved by comparison with the load-deformation curve obtained from the experimental results. Then the validations of the assumed shape function and the elastic buckling strength equation will be discussed in article 4.3.2 and 4.3.3, respectively.

4.3.1. Establishment of finite element analysis model

Material properties

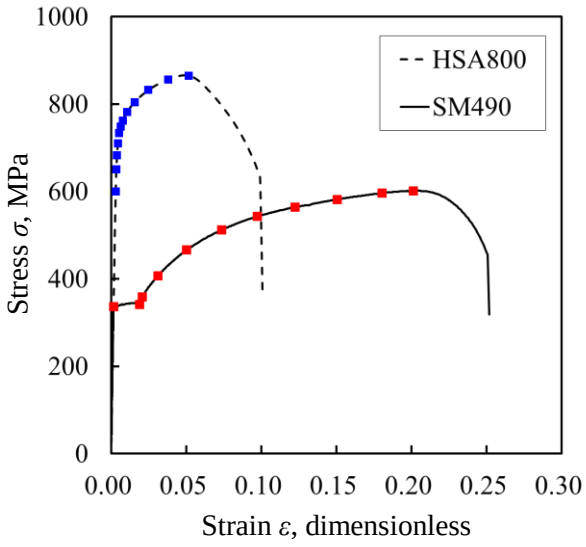

Figure 4.7 Stress-strain curve of tensile test and data for numerical analysis

Figure 4.7 shows the stress-strain curves obtained from tensile test results. The curves were obtained from one of the material tests done for SM490 and

HSA800. From this graph, the yield stress and plastic strain data is collected to apply on numerical analysis. The collected data is shown in Table 4.3. The data in this Table was used to increase the accuracy of the analysis simulating the post-elastic behavior of the material and the analysis models.

Table 4.3 Yield stress and plastic strain applied in numerical analysis

Data	**SM490 (ordinary steel)**		**HSA800 (high-strength steel)**	
	Yield stress, MPa	Plastic strain, dimensionless	Yield stress, MPa	Plastic strain, dimensionless
1	336.4899	0	600.4089	0
2	340.699	0.017493	650.6953	0.000421
3	359.0531	0.019147	682.3573	0.000825
4	406.5352	0.029502	710.0799	0.001463
5	465.7334	0.048633	732.9557	0.002334
6	511.7087	0.072105	748.3549	0.003266
7	542.6111	0.09589	762.0667	0.004632
8	564.0034	0.121073	781.5816	0.007543
9	581.6204	0.14895	804.0899	0.012509
10	596.0511	0.178815	832.0685	0.02182
11	601.493	0.199643	856.5803	0.034904
12	-	-	865.1321	0.048724

Analysis conditions

For this investigation, the numerical analysis models were established as the following conditions:

1. The element type of the models was solid and 20-nodes element integrated by reduced integration.

2. The lower and upper ends of the braces were fixed by supported condition in the ABAQUS software, restrained by six degrees of freedom. The *x*, *y* and *z* direction displacements (represented by U1, U2 and U3 in analysis software) and rotations (represented by R1, R2 and R3 in analysis software) are set to be zero value.
3. Riks analysis was done to simulate the experiments of β = 1 RHS X-joints under axial compression.

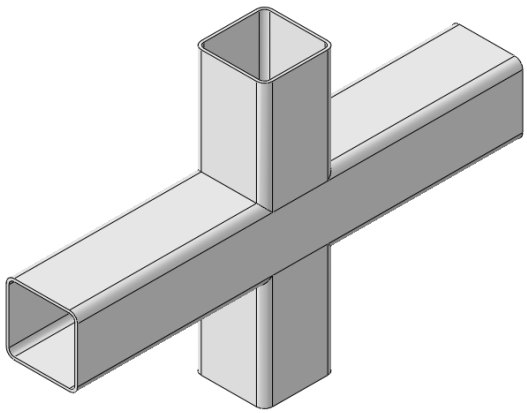

Figure 4.8 Finite element analysis model of β = 1 RHS X-joints

Result comparison

From numerical analysis results shown in Figure 4.9, relations of applied compressive force versus normalized indentation were obtained. In elastic range of RHS X-joints, regardless of steel grades, experimental result and numerical analysis result correspond to each other. However, the curves obtained by numerical analysis had the peak strength values slightly lower than the peak strengths of experimental results. Furthermore, the curves

obtained by numerical analysis lost its strength more rapidly than the strength curves of experimental results.

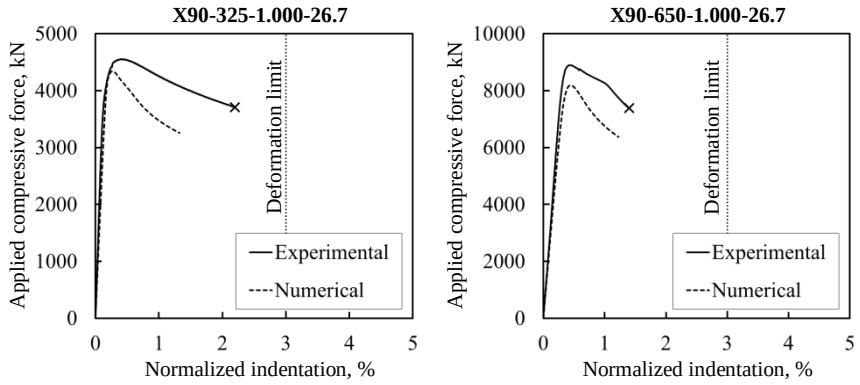

Figure 4.9 Compressive force versus normalized indentation relationships for both experimental and numerical analysis results

Table 4.4 shows the comparison between the experimental results and the numerical analysis results. The peak strength values of experimental results were 4553 kN and 8895 kN for SM490 and HSA800, respectively, while the peak strengths obtained from numerical analysis were 4341 kN and 8188 kN for ordinary steel and high-strength steel, respectively. These results just show the error within 8%.

Table 4.4 Comparison between experimental and numerical analysis results

Specimen	Experimental		Numerical		Peak load error, %
	Indentation, %	Load, kN	Indentation, %	Load, kN	
X90-325-1.000-26.7	0.403	4553	0.275	4341	4.66
X90-650-1.000-26.7	0.433	8895	0.447	8188	7.95

Since the welding parts were not included in these numerical analysis

models, the peak strengths of numerical analysis results are slightly (about 10%) less than the strength obtained from experimental results. It is just a conservative result with negligible difference that these models could be used for eigenvalue analysis.

Therefore, the numerical models and their analysis conditions could be regarded as reasonable. In the later articles, these conditions are applied on eigenvalue analysis to obtain the elastic buckling strength of β = 1 RHS X-joints.

4.3.2. Validation of assumed shape function

Numerical analysis program

This analysis was done by RHS X-joints model with different geometries. The key parameter of this analysis program is h_1 over b_1, the aspect ratio of the brace sections which could controls the strength of the restraint effect caused by the welded braces.

Table 4.5 Numerical analysis program

Model		1	2	3
t_0 and t_1, mm		15		
Chord section	b_0, mm	250		
	$\lambda = (b_0-2t_0)/t_0$, dimensionless	14.7		
Brace section	h_1, mm	125	250	500
	$\lambda = (h_1-2t_1)/t_1$, dimensionless	6.3	14.7	31.3
Section classification		Class 2		

NOTE: 1. Class 2 requirement: $\lambda \leq 32.3$
2. $f_{y0} = f_{y1}$ = 325 MPa

The numerical analysis program is shown in Table 4.5. Because EC3

restrained the aspect ratio of the brace section h_1 / b_1 in the range of 0.5 to 2, the analysis models were conducted to satisfy this limitation.

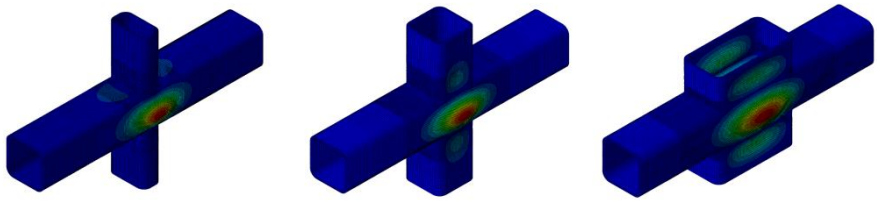

Figure 4.10 General views of numerical eigenvalue analysis results (deformation amplification factor: 50)

Figure 4.10 shows the general views for the deformed shapes of the model analyzed by numerical analysis. As a red area show the deformation close to unity, the deformations caused by buckling are concentrated at the center of the chord for these analysis models.

Shape data obtained from FEA eigenvalue analysis

Three deformed shapes of each eigenvalue analysis result were plotted to be compared with the assumed shape function. These shapes were measured to investigate the restraint effect of braces which resist the out-of-plane deformation of chord sidewalls. Obtained buckling shape functions were numerically differentiated by Central Difference Method. The equations of Central Difference Method for slope and curvature of deformed shape at x_i distance from zero point are shown as the following equations:

$$f'(x_i) = \frac{f(x_{i+1}) - f(x_{i-1})}{2(x_{i+1} - x_{i-1})} \quad f''(x_i) = \frac{f(x_{i+1}) - 2f(x_i) + f(x_{i-1})}{(x_{i+1} - x_{i-1})^2} \quad (4.21)$$

where $f(x_i)$ is the deformed shape obtained from FEA at x_i

As the distance from the brace walls on the planes orthogonal to the longitudinal direction of the chord become larger, the resisting strengths caused by the brace walls are getting less. Thus, at the center of the chord, the weakest restraint effects caused by the braces width direction walls are induced. The deformed shapes at the weakest part of chord sidewalls will be shown in the following paragraphs.

Deformed shapes visualized by finite element analysis program (ABAQUS) are shown in Figure 4.11 through 4.13. The deformed shapes obtained by FEM eigenvalue analysis are represented by eigenvector whose maximum value is unity.

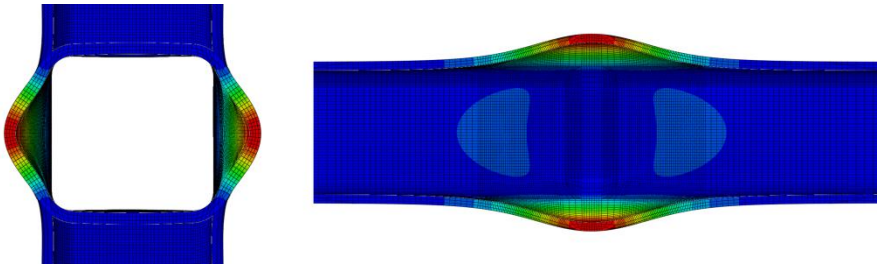

Figure 4.11 Deformed shape of transverse and longitudinal cross section obtained from FEA eigenvalue analysis with $h_1/b_1 = 0.5$ (deformation amplifying factor: 50)

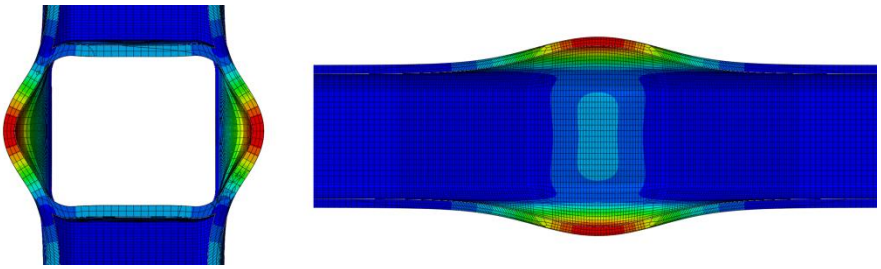

Figure 4.12 Deformed shape of transverse and longitudinal cross section obtained from eigenvalue analysis of FEA model with $h_1/b_1 = 1$ (deformation amplifying factor: 50)

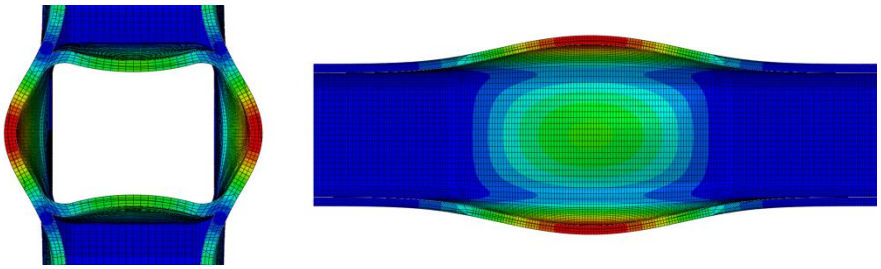

Figure 4.13 Deformed shape of transverse and longitudinal cross section obtained from eigenvalue analysis of FEA model with $h_1/b_1 = 2$ (deformation amplifying factor: 50)

As shown in Figures 4.11, 4.12 and 4.13, the deformations occurred at the chord upper and lower faces are getting larger with increment of h_1/b_1. As a consequence, with relatively large value of h_1-b_1 ratio, the support conditions of chord sidewalls in transverse direction become similar to simply supported rather than fixed supported. This proposition will be investigated in the later paragraph.

Buckled shape and its 1st and 2nd derivatives obtained from FEA eigenvalue analysis

For analysis model with $h_1/b_1 = 0.5$, the restraint effects of the braces is the strongest among these analysis models. The model which the weakest restraint effects acted on the chord sidewall is the one with $h_1/b_1 = 2$. It is clearly observed that the supported conditions of chord sidewalls for the transverse direction of the chord are in between fixed support condition and hinged support condition. However, it is shown to be much closer to fixed than hinged. The deformed shape function obtained from numerical analysis and its 1st and 2nd derivatives calculated by numerical differentiation will be shown in Figure 4.14 through 4.16.

i. Analysis model with h_1/b_1 = 0.5

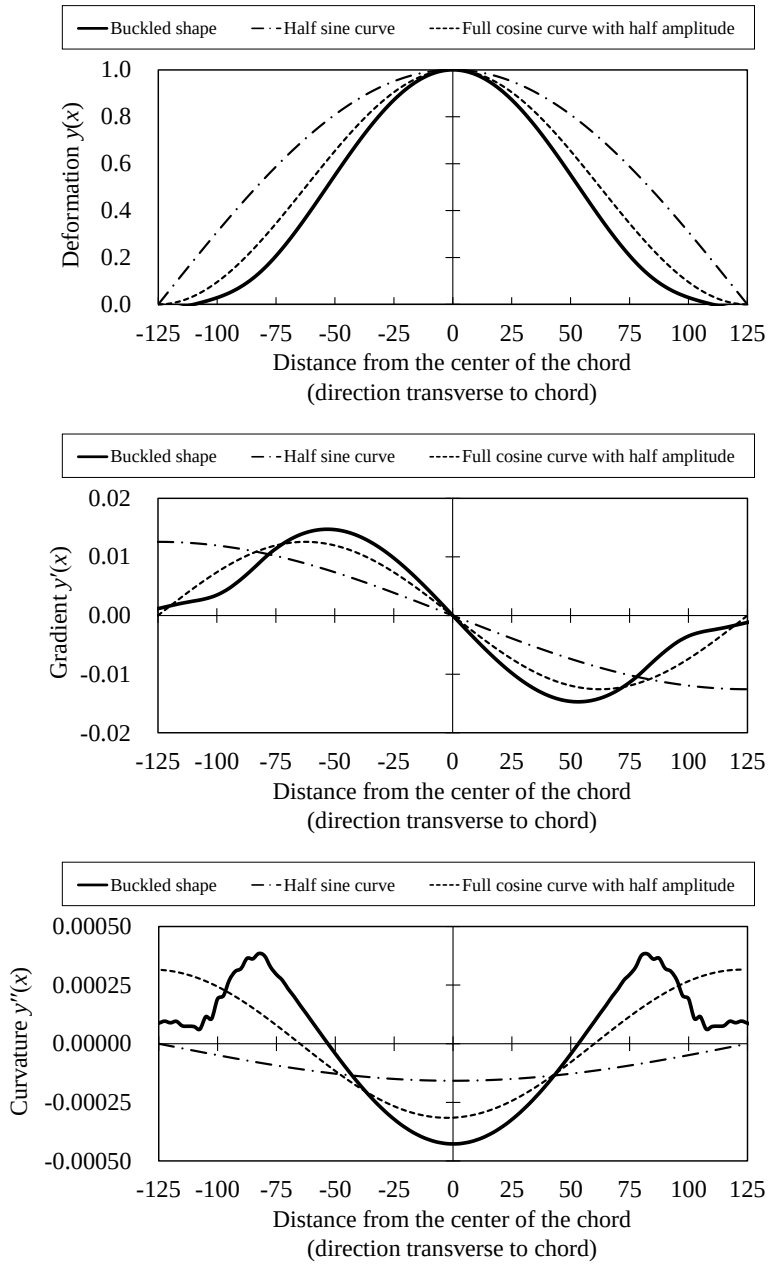

Figure 4.14 Buckled shape and its 1st and 2nd derivatives compared with half sine curve and full cosine curve with half amplitude (h_1-b_1 ratio: 0.5)

ii. Analysis model with h_1/b_1 = 1-

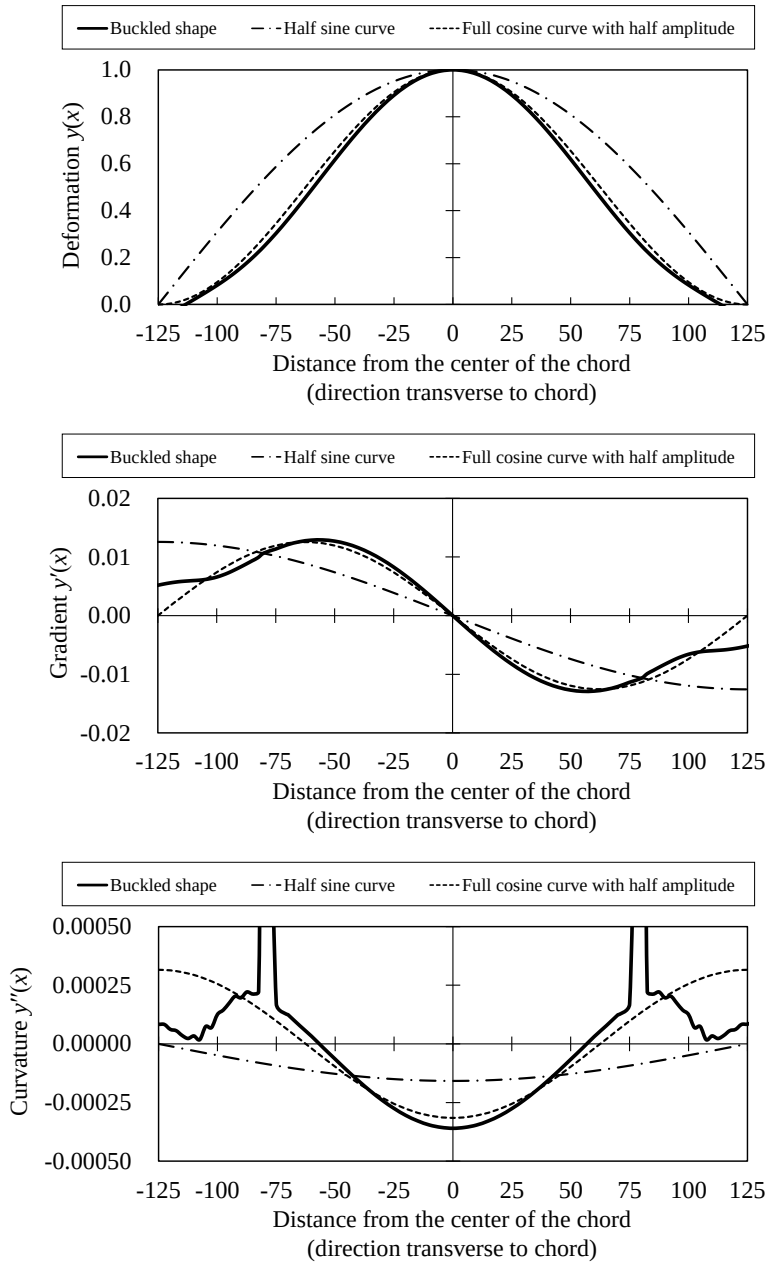

Figure 4.15 Buckled shape and its 1st and 2nd derivatives compared with half sine curve and full cosine curve with half amplitude (h_1-b_1 ratio: 1)

iii. Analysis model with $h_1/b_1 = 2$

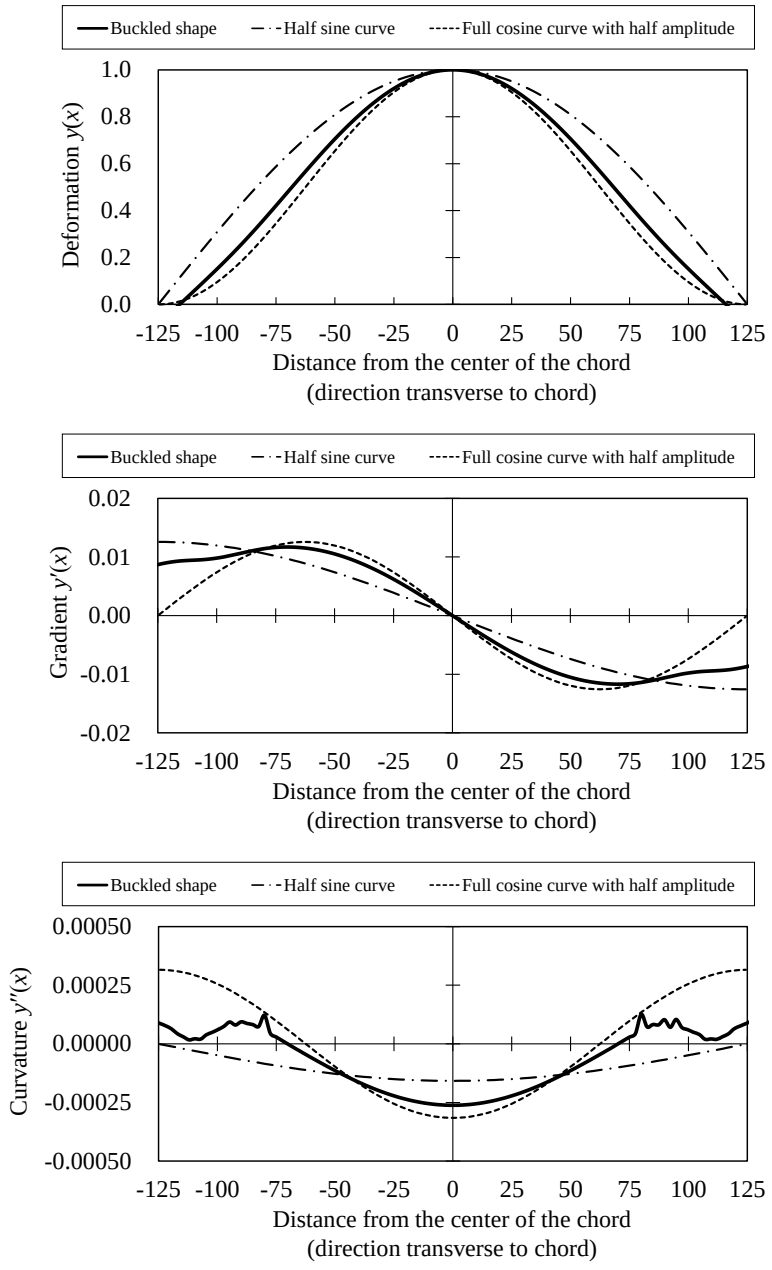

Figure 4.16 Buckled shape and its 1st and 2nd derivatives compared with half sine curve and full cosine curve with half amplitude (h_1-b_1 ratio: 2)

4.3.3. Validation of elastic buckling strength equation

To validate the elastic buckling strength equations obtained from theoretical models, numerical analysis programs were conducted with the key parameters. A aspect ratio of brace section, h_1/b_1 was set as a key parameter of a numerical program that controls the strength of restraint effects caused by braces. FEM eigenvalue analysis with this parameter could show the accuracy of the elastic buckling strength equations depending on restraint effects. In the other numerical analysis program, thicknesses of brace and chord section t_0 and t_1 identical to each other are used as a key variable. This parameter was used to investigate the scale effect that could be caused by thicknesses of sections.

For different h_1-b_1 ratio

Table 4.6 Elastic buckling strengths obtained from different theoretical models and comparison with FEA results (Parameter: h_1/b_1)

Index	**Model**			
h_1-b_1 ratio	Proposed model	Becque's model	Simplistic column model	FEA result
	Buckling load, kN			
0.5	18055 (72.1%)	6733 (26.9%)	4703 (18.8%)	25036 (100%)
1	26221 (84.6%)	6733 (21.7%)	7642 (24.7%)	30986 (100%)
2	44688 (132.6%)	6733 (20.0%)	13521 (40.1%)	33692 (100%)

*NOTE: Data in parentheses shows the elastic buckling strength normalized by the strength obtained from FEA results.

Table 4.6 in article 4.3.2 showed the FEM eigenvalue analysis to simulate the actual behavior of RHS X-joints with equal-width. Using the identical models mentioned in previous article, the elastic buckling strengths could be obtained

from FEA results. The elastic buckling strengths obtained from the other theoretical models were reported in Table 4.6. The results of FEM eigenvalue analysis are shown in Figure 4.17 with the elastic buckling strengths of theoretical models. The parameter of this analysis was h_1/b_1.

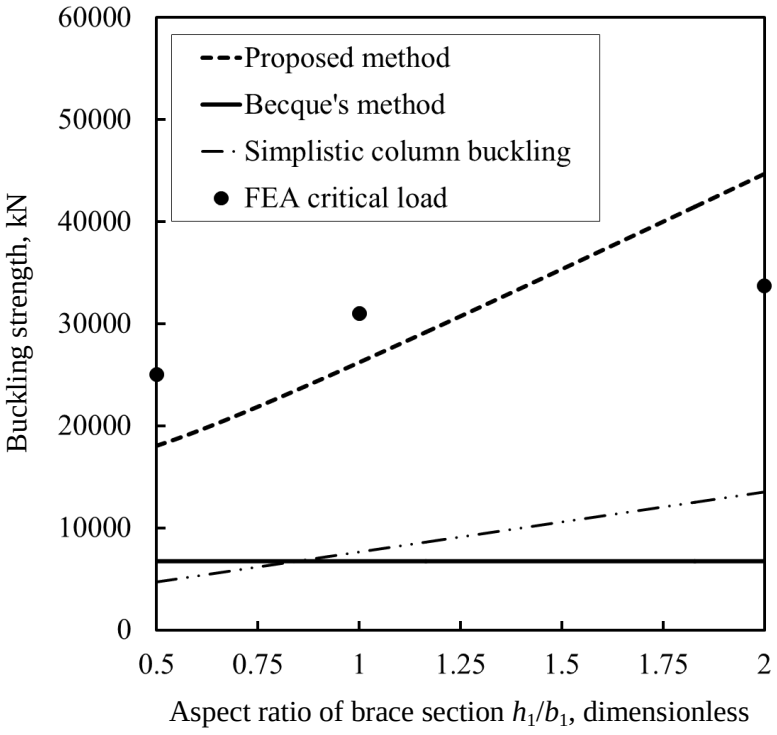

Figure 4.17 Comparative analysis of FEM eigenvalue analysis results with elastic buckling strengths of theoretical models (parameter: h_1/b_1)

For different thicknesses

Buckled shapes are determined by the relative flexural stiffness between the braces and the chord sidewall. Thus, the numerical analysis models were conducted to verify this statement. In this paragraph, the elastic buckling strengths obtained from the eigenvalue analysis for different thicknesses with

same thickness ratio between sections of a chord and braces ($t_0 = t_1$, where t_0 is the thickness of the chord section and t_1 is the thickness of the brace section) were compared with different elastic buckling strength equations of $\beta = 1$ RHS X-joints.

Table 4.7 shows the numerical analysis program conducted to obtain elastic buckling strengths. Identical geometric configuration of experimental specimen with $\beta = 1$ was applied to these models. Only difference between these models and experimental specimen was the thicknesses of sections.

Table 4.7 Numerical analysis program to obtain elastic buckling strength

Model number		1	2	3	4
Brace and chord section	b_i and h_i, mm	400			
	t_i, mm	12	15	18	25
	$(b_i\text{-}2t_i)/t_i$	31.3	24.7	20.2	14.0

*NOTE: Subscript i: 0 for a chord section and 1 for a brace section

Figure 4.18 shows the results of FEM eigenvalue analysis. As shown in this Figure, the elastic buckling strengths of simplistic column derived in Wardenier (1982) and plate model established in Becque and Cheng (2016) underestimate and also inaccurately predict the elastic buckling strength of $\beta = 1$ RHS X-joints. On the other hand, the elastic buckling formula derived in this chapter slightly underestimate the elastic buckling strength of $\beta = 1$ RHS X-joints. Table 4.8 shows the elastic buckling strengths obtained from different theoretical models compared with FEA results.

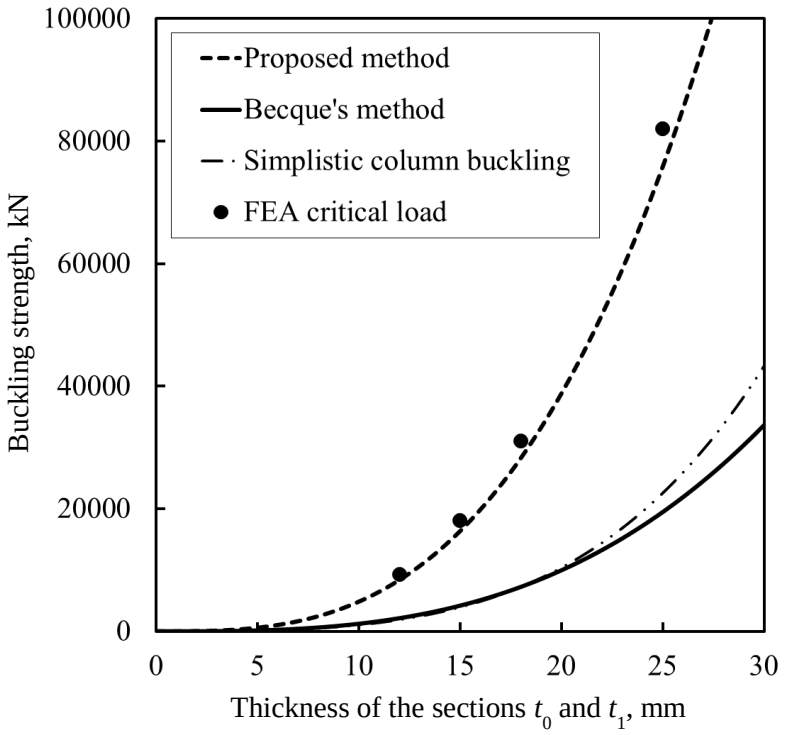

Figure 4.18 Comparative analysis of FEM eigenvalue analysis results with elastic buckling strengths of theoretical models (parameter: t_0 (=t_1))

Table 4.8 Elastic buckling strengths obtained from different theoretical models and comparison with FEA results (parameter: t_0 (=t_1))

Index	**Model**			
t_0=t_1, mm	Proposed model	Becque's model	Simplistic column model	FEA result
	Buckling load, kN			
12	8391 (89.8%)	2155 (23.1%)	1896 (20.3%)	9345 (100%)
15	16388 (90.6%)	4208 (23.3%)	3949 (21.8%)	18087 (100%)
18	28319 (91.1%)	7272 (23.4%)	7273 (23.4%)	31071 (100%)
25	75871 (92.5%)	19483 (23.8%)	22581 (27.5%)	82027 (100%)

*NOTE: Data in parentheses shows the elastic buckling strength normalized by the strength obtained from FEA results.

4.4. Proposal of new sidewall buckling strength formula

The derivation and the validation of the alternative design method were done in the previous clauses. As a consequence, the new equation of sidewall buckling failure mode derived in this thesis will be introduced here. In this section, the elastic buckling strength and the yielding strength of the chord sidewall are determined as accurately as possible such that normalized plate slenderness ratio could be obtained reasonably. Then, the evaluation of this method was done by β = 1 RHS X-joints database collected from available literatures.

4.4.1. Derivation of slenderness ratio

The slenderness of β = 1 RHS X-joints to consider an inelastic behavior could be derived by its definition:

$$\lambda = \sqrt{\frac{N_y}{N_{cr}}} \tag{4.22}$$

where N_y and N_{cr} is the yield strength and the elastic buckling strength of β = 1 RHS X-joints, respectively. Thus, the yield strength and the elastic buckling strength should be determined to obtain the slenderness ratio of β = 1 RHS X-joints.

Yield strength of β = 1.0 RHS X-joints

As shown in Figure 4.19, the load is applied on the braces. The strength of chord sidewall yielding in area compressed by braces N_y could be expressed

as the following equation:

$$N_y = 2 f_{y0} h_1 t_0 \tag{4.23}$$

where f_{y0} is the yield stress of chord member, h_1 is the height of the section of the braces and t_0 is the thickness of the chord section.

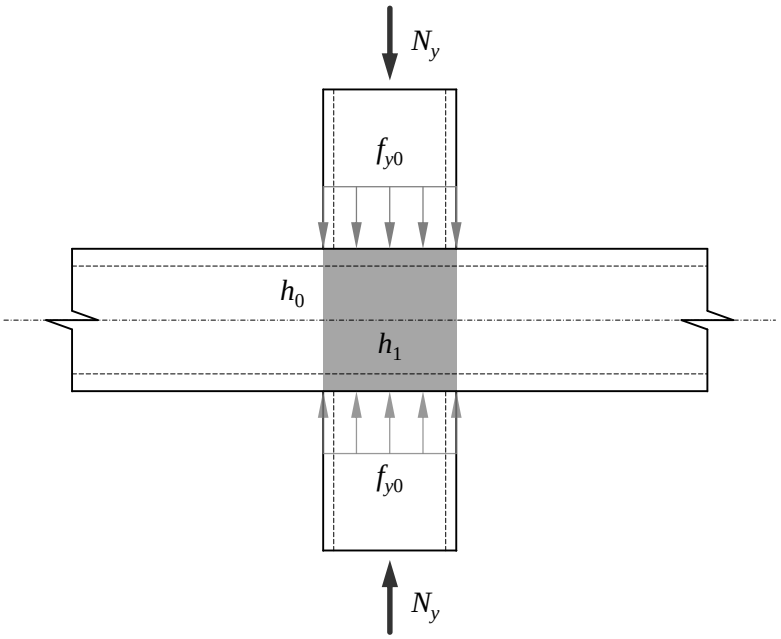

Figure 4.19 β = 1 RHS X-joints chord sidewalls loaded by force P_y transferred from braces

For the new design method, yield strength equation is modified as shown in the equation:

$$N_{proposed,y} = 1.2 N_y = 1.2 \times \left(2 f_{y0} h_1 t_0 \right) = 2.4 f_{y0} h_1 t_0 \tag{4.24}$$

The factor of 1.2 thereby takes into account that a small part of a load follows an alternative load path through chord top and bottom faces, and spreads onto chord sidewalls. This factor was suggested in the work of Becque and Cheng

(2016)

New elastic buckling strength equation

The elastic stress derived in the previous section is repeated in here.

$$\sigma_{cr} = 5.2415 \cdot e^{0.32(h_0/h_1-1)} \cdot \frac{\pi^2 E}{12\left(1-\nu^2\right)} \frac{t_0^2}{h_0^2}$$

Then the elastic strength equation of β = 1 RHS X-joints could be obtained as shown below:

$$N_{cr} = \sigma_{cr} A = \left[5.2415 \cdot e^{0.32(h_0/h_1-1)} \cdot \frac{\pi^2 E}{12\left(1-\nu^2\right)} \frac{t_0^2}{h_0^2} \right] \cdot 2t_0 h_1$$

$$\therefore N_{cr} = 10.483 \cdot e^{0.32(h_0/h_1-1)} \cdot \frac{\pi^2 E}{12\left(1-\nu^2\right)} \frac{h_1 t_0^3}{h_0^2} = 2k \frac{h_1}{h_0} \cdot \frac{\pi^2 D}{h_0} \qquad (4.25)$$

where D is a flexural rigidity of the plate defined as $Et_0^3/(12(1-\nu^2))$ and k is a numerical factor obtained in section 4.2.4 by MATLAB program which could be expressed as $5.2415 \cdot \exp[0.32(h_0/h_1-1)]$. A height ratio between a chord and braces h_1/h_0 considers the influence of restraints caused by braces.

Slenderness ratio

As equation 4.22 in the beginning of this article, the slenderness ratio could be given by:

$$\lambda = \sqrt{\frac{N_y}{N_{cr}}} = \sqrt{\frac{2.4 f_{y0} h_1 t_0}{10.483 \cdot e^{0.32(h_0/h_1-1)} \cdot \frac{\pi^2 E}{12\left(1-\nu^2\right)} \frac{h_1 t_0^3}{h_0^2}}}$$

$$\therefore \lambda = 1.6575 \cdot e^{-0.16(h_0/h_1-1)} \frac{h_0}{t_0} \cdot \frac{\sqrt{1-\nu^2}}{\pi} \sqrt{\frac{f_{y0}}{E}} \tag{4.26}$$

where h_0 is the height of the chord section, h_1 is the height of the brace section, t_0 is the thickness of the chord section, v is Poisson's ratio (generally, the value of 0.3 is used.), f_{y0} is the yield stress of the chord and E is the elastic ratio of the steel. If the value of 0.3 for v is used, the slenderness ratio λ yields to:

$$\lambda = 1.581 \cdot e^{-0.16(h_0/h_1-1)} \cdot \frac{1}{\pi} \sqrt{\frac{f_{y0}}{E}} \cdot \frac{h_0}{t_0} \tag{4.27}$$

for E = 205000 MPa, the equation could be simplified as:

$$\lambda = \frac{1}{899.61} e^{-0.16(h_0/h_1-1)} \frac{h_0}{t_0} \sqrt{f_{y0}} \approx \frac{1}{900} e^{-0.16(h_0/h_1-1)} \frac{h_0}{t_0} \sqrt{f_{y0}} \tag{4.28}$$

4.4.2. Derivation of chord sidewall buckling strength formula

As suggested in Becque and Cheng (2016), inelastic buckling strength of β = 1 RHS X-joints could be obtained by the yield strength equation multiplied by the buckling stress reduction factor χ. Thus, the equation proposed in this section could be expressed by:

$$N_{cr} = 2.4 \chi f_{y0} h_1 t_0 \tag{4.29}$$

where χ is the buckling stress reduction factor, f_{y0} is the yield stress of the chord section, h_1 is the height of the brace section and t_0 is the thickness of the chord section.

This equation implies the nature of buckling behaviors. Inelastic

buckling strength could not exceed the yield strength since the range of the buckling stress reduction factor χ is zero to unity. Therefore, for the maximum value of χ, the equation of N_{cr} yields to be the identical equation of N_y.

To determine the buckling strength reduction factor, the slenderness ratio λ derived in the previous section should be applied to the buckling curve. The proposed method recommends using "c" curve of EC3 multiple curves which is used to determine χ value in EC3 chord sidewall buckling strength formula.

4.4.3. Evaluation of new joint strength formula

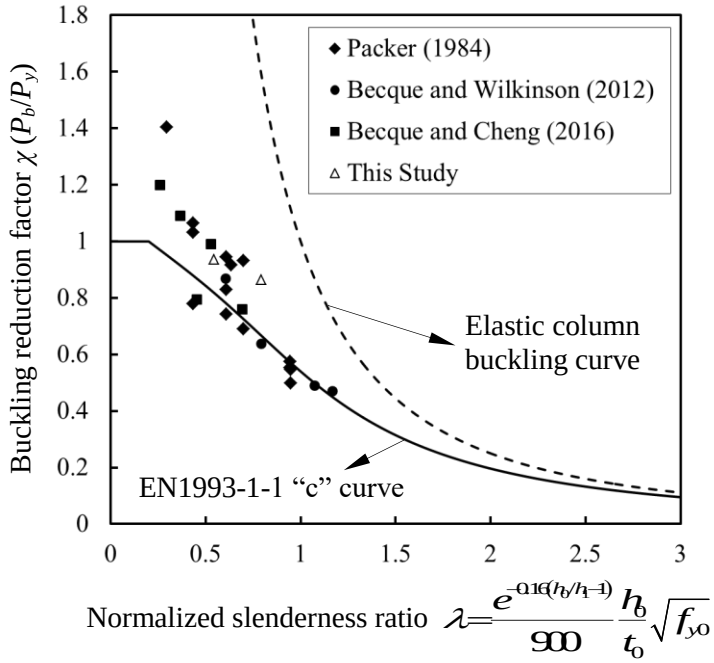

Figure 4.20 Relationship between buckling stress reduction factor and normalized slenderness ratio

As a result, comparative analysis of the new joint strength formula was done by database collected in previous experimental studies. Figure 4.20 shows the

results of comparative analysis. Dotted line is elastic column buckling curve which is inversely proportional to normalized slenderness ratio, and solid line is "c" curve of the multiple curves suggested in Eurocode3 (2005)

The experimental strength normalized by the sidewall buckling strength derived in this thesis (N_{exp} / N_b) is used to evaluate the results. Table 4.9 shows the statistic parameters of this comparison.

Table 4.9 Statistic parameters of the comparative analysis

N_{exp} / N_b	Maximum	minimum	Mean	MSE	COV
	1.48	0.87	1.09	0.17	0.16

Since the true value of this normalized experimental strength is unity, mean square error which could express the deviation of this method could be calculated by its definition:

$$\mathrm{MSE} = \frac{1}{n}\sum_{i=1}^{n}\left(y_i - \tilde{y}_i\right)^2 \tag{4.30}$$

where y_i is the normalized experimental strength of one specimen in database and $\tilde{y}_i$ is the true value 1 when the experimental strength N_{exp} is equal to the design strength N_b. COV is the coefficient of variation which could be calculated by the following equation:

$$\mathrm{COV} = \frac{\sigma}{m} \tag{4.31}$$

where σ is the standard deviation and m is the mean value.

The maximum and minimum values of normalized experimental strength

are 1.48 and 0.87, respectively. The mean value of N_{cr}/N_b is 1.09 which means that newly suggested strength equation only underestimate the experimental strength about 9%. Mean square error value representing the deviation of N_{cr}/N_b obtained by the new sidewall buckling strength equation is the least value among current design equations. Also COV, which represents dispersion of data, is the minimum value among the other methods.

4.5. Summary

1. The sidewall buckling formula proposed by the plate buckling model predicts the strength more accurately than by the simplistic column buckling model. But the equation of Becque and Cheng still conservatively predicts the experimental strengths of RHS X-joints fabricated from high-strength steels.
2. The boundary condition of the chord sidewall was shown to be much closer to fixed than hinged. In order to define more reasonable normalized plate slenderness, therefore, fixed boundary conditions were used to derive elastic buckling strength formula of the chord sidewall by the Work Method.
3. When the new normalized slenderness ratio proposed in this study is used in combination with the curve “c” of EC3, the accuracy and consistency in strength predictions was much improved compared to other methods available.

Chapter 5

Summary and Conclusions

In this thesis, the behavior of rectangular hollow section (RHS) X-joints was investigated by experimental, analytical and numerical analysis. Most of RHS X-joints with general geometries are governed by the failure modes of chord plastification, chord sidewall buckling and the mixed mode of these two modes.

These failure modes are determined by transfer mechanisms of loads which come from braces, distributed to chord upper/lower face. Load transfer mechanisms are mainly governed by a geometric parameter β, a width ratio between braces and a chord. Therefore, the value of β was set to key parameter in experimental study.

Another key parameter was grades of steels. From design to construction of structures, applying high-strength steel to rectangular hollow section joints can be an effective way to reduce total amount of structural steel and to give an aesthetic view to the buildings. Despite of these benefits, RHS X-joints

fabricated from high-strength steel whose yield stress exceeds 355 MPa are restricted in KBC (2016) and AISC (2010). Eurocode3 (2005) which gives quite general design standards for high-strength steels, suggests multiplying the strength reduction factor of 0.8 or 0.9 to the nominal strength formula of RHS X-joints fabricated from high-strength steel.

To examine the penalty imposed on high-strength steels, six test specimens those consist of cold-formed channel sections fabricated from high-strength steel (HSA800, f_y = 650 MPa) and ordinary steel (SM490, f_y = 325 MPa) were tested under axial compression. The strengths of test specimens were determined by the maximum strength within 3% indentation, widely-accepted criteria. As a result of the experiment, all of the high-strength steel RHS X-joint specimens satisfied EC3's nominal strength with sufficient margin. Also, the experimental strengths exceeded the strength before applying strength reduction factor 0.8. Overall, RHS X-joints with high-strength steel show satisfactory performances just slightly inferior to that of the X-joints fabricated from ordinary steel, in respect to their ductility and serviceability. However, it is clearly shown that the strength of β = 1 RHS X-joints determined by sidewall buckling strength equations suggested in current EC3 and CIDECT, originally proposed based on simply supported column analogy, are too conservative and need to be improved.

After collecting test data available in the literature and this experimental program, a comparative analysis was conducted to compare the experimental strengths with Eurocode3, AISC and the formula proposed by Becque and Cheng. The sidewall buckling formula proposed by the plate buckling model

predicts the strength more accurately than by the simplistic column buckling model, but it is still inaccurate. AISC strength equation shows the largest scatter among these equations which could overestimate the actual strengths. Becque-Cheng's method gives more reliable strengths but it is still too conservative for the joints fabricated from high-strength steels.

Numerical analysis models were established with boundary conditions validated by load-indentation relations obtained from the experimental results. Eigenvalue analysis with FEA models was conducted to determine the reasonable and simple shape functions. From these results, the boundary conditions of the chord sidewall were shown to be much closer to fixed than hinged. By using the buckled shape function which is consistent with this observation, the elastic buckling strength formula of the chord sidewall was obtained using the Work Method in order to define more reasonable normalized plate slenderness. When the proposed normalized slenderness ratio is used in combination with "c" curve of EC3 multiple buckling curves, the accuracy and consistency of strength predictions were much improved compared to other methods available.

Bibliography

[1] AISC. (2010). *Specification for Structural Steel Buildings*: American Institute of Steel Construction.

[2] Becque, J., and Cheng, S. (2016). Sidewall Buckling of Equal-Width RHS Truss X-Joints. *Journal of Structural Engineering, 143*(2), 04016179.

[3] Becque, J., and Wilkinson, T. (2012). *Experimental investigation of the static capacity of grade C450 RHS T and X truss joints.* Paper presented at the Proceedings of the 14th International Symposium on Tubular Structures. London.

[4] Chen, W.-F., and Newlin, D. E. (1971). Column web strength in steel beam-to-column connections (ASCE Meeting reprint 1524).

[5] Chen, W., and Oppenheim, I. (1970). *Web Buckling Strength of Beam-to-Column Connections Fritz Engineering Laboratory*. Retrieved from

[6] CIDECT. (1992). Design Guide for Rectangular Hollow Section (RHS) Joints Under Predominantly Static Loading. In: TUV-Verlag GmbH.

[7] CIDECT. (2009). *Design Guide for Rectangular Hollow Section (RHS) Joints Under Predominantly Static Loading*: CIDECT.

[8] Eurocode3. (2005). *EN 1993-1-8: Eurocode 3: Design of Steel Structures. Part 1-8: Design of joints*: Comité Europeo de Normalización.

[9] IIW. (1981). *International Institute of Welding Subcommission XV-E: Design Recommendations for Hollow Section Joints - Predominantly Statically Loaded* (2nd ed.). Oporto, Portugal: International Institute of Welding Annual Assembly.

[10] KBC. (2016). Korean Building Codes and Commentay. In (2nd edition ed.). Seoul: Kimoondang.

[11] Kurobane, Y. (1981). New developments and practices in tubular joint design. *Memoirs of the Faculty of Engineering, Kumamoto University, 26*(1), 1-57.

[12] Lu, L., De Winkel, G., Yu, Y., and Wardenier, J. (1994). *Deformation limit for the ultimate strength of hollow section joints.* Paper presented at the 6th International Symposium on Tubular Structures.

[13] Noordhoek, C., Verheul, A., Foeken, R., Bolt, H., and Wicks, P. (1996). Static strength of high strength steel tubular joints. *ECSC agreement number 7210-MC, 602*.

[14] Packer, J. A. (1984). Web crippling of rectangular hollow sections. *Journal of Structural Engineering, 110*(10), 2357-2373.

[15] Packer, J. A. (1987). Review of American RHS web crippling provisions. *Journal of Structural Engineering, 113*(12), 2508-2513.

[16] Puthli, R., Bucak, O., Herion, S., Fleischer, O., Fischl, A., and Josat, O. (2010). *Adaptation and extension of the valid design formulae for joints made of high-strengths steels up to S690 for cold-formed and hot-rolled*

sections (5BT-7/10). Retrieved from

[17] Timoshenko, S., and Gere, J. M. (1961). *Theory of elastic stability*. New York: McGraw-Hill.

[18] Wardenier, J. (1982). *Hollow section joints*. Delft: Delft University Press.

Appendix A

MATLAB Source Codes to Calculate Buckling Stress

1. Main function, 'Plate_Buckling.m' source code

```
clear;

% Variables declaration
global alpha

% Variables initialization
q_crs = zeros(5001,1);
alpha_s = zeros(5001,1);
c_s = zeros(5001,1);

% 'for' command to solve nonlinear equation
% Variable alpha is in the range of (0.25 <= alpha <= 4)
for count = 1:5001
```

```
    alpha = 0.25 + ((4 - 0.25) / 5000) * (count - 1);

    % alpha solution value assignment
    alpha_s(count) = alpha;

    % c solve
    c = fsolve(@PB, 1);

    % Assignment of solved c value
    c_s(count) = c;

    % q_cr calculation
    q_crs(count) = (9 / (16 * (pi^4))) * (c^4) + ( 1 / (pi^2) ) * (c ^2) + 4;
    q_crs(count) = q_crs(count) / erf(alpha * c / 2);
end

disp('Solution Obtained')
```

2. Main function, 'Plate_Buckling.m' source code

```
function = PB

global alpha;
```

```
LL = ( alpha * exp( - (alpha^2 * c^2) / 4) ) / (sqrt(pi) * erf( alpha * c / 2));
RR = ( 36 * (c^3) + 32 * (pi^2) * c ) / (9 * (c^4) + 16 * (pi^2) * (c^2) + 64 *
(pi^4));

difference = RR - LL;
end
```

Abstract (in Korean)

최근 건축물은 물론 해양구조물에도 적용되는 강관은 기둥과 트러스로 널리 사용되고 있다. 그중에서 각형강관은 강관의 제작과 용접이 간단하여 원형강관을 대체하는 단면으로 활용되고 있다. 각형강관에 고강도강관을 사용하면 설계부터 제작, 운반, 시공뿐 아니라 미학적 측면으로도 많은 이점을 취할 수 있다. 그러나 고강도 강재를 적용하는 데 있어 가장 관대한 기준인 유로코드에서조차 고강도 강재를 적용한 각형강관 접합부의 강도를 산정할 때에는 사용되는 강재의 항복강도에 따라 0.8 또는 0.9의 강도감소계수를 곱하도록 제한하고 있다.

본 연구에서는 유로코드에서 제안하는 강도감소계수의 적절성을 검증하기 위해 각형강관 X형 접합부에 압축력을 가하는 실험을 계획하였다. 실험변수는 2가지로 강재의 항복강도(f_y)와 지관과 주관 사이의 폭 비율(β)이다. 총 6개의 실험체를 제작하였으며, 실험결과, 접합부의 탄성구간 이후 거동은 지관과 주관의 폭 비율에 따라 굉장한 차이를 보였다. 모든 실험체가 유로코드 공칭강도를 초과하는 실험강도를 보였으며, 발현된 실험강도들은 0.8의 강도감소계수가 적용되지 않은 유로코드 공칭강도조차도 상회하였다. 한편, 지관과 주관의 폭이 동일한 X형 접합부 실험체에 적용되는 주관측벽 좌굴강도식은 실험강도를 지나치게 보수적으로 예측하였기에 그 정확도를 개선해야한다. 선행연구 중에는 개선된 주관측벽 좌굴강도식을 제안하는 연구도 있었으나, 이 연구에서

제안한 식을 통해 얻은 예측강도는 고강도 강재를 적용한 실험체의 강도를 여전히 보수적으로 평가하였다.

그러므로 본 연구에서는 새로운 주관측벽 좌굴강도식을 제안하였다. 이 식은 판 좌굴에 근거한 이론적 모델에서 유도되었으며, 수치해석을 통해 그 유효성을 검증하였다. 또한, 선행 연구들로부터 수집한 실험강도 데이터를 통해 본 연구에서 제시한 식과 현행 주관측벽 좌굴강도식들을 비교하였다. 결론적으로, 본 연구에서 새롭게 정의한 세장비를 유로코드 기둥좌굴 곡선 중 하나인 “c”곡선에 적용한다면 현존하는 다른 강도식보다 더 일관성 있고 정확한 예측강도를 얻을 수 있다.

주요어: 각형강관; X형 접합부; 고강도 강재; 극한강도식; 실대형 실험